Multi-Contact Bipedal Robotic Locomotion

Huihua Zhao, Ayonga Hereid, Wen-loong Ma and Aaron D. Ames

Abstract

This paper presents a formal framework for achieving multi-contact bipedal robotic walking, and realizes this methodology experimentally on two robotic platforms: AMBER2 and ATRIAS. Inspired by the key feature encoded in human walking—multi-contact behavior—this approach begins with the analysis of human locomotion and uses it to motivate the construction of a hybrid system model representing a multi-contact robotic walking gait. Human-inspired outputs are extracted from reference locomotion data to characterize the human model or the SLIP model, and then employed to develop the human-inspired control and an optimization problem that yields stable multi-domain walking. Through a trajectory reconstruction strategy motivated by the process that generates the walking gait, the mathematical constructions are successfully translated to the two physical robots experimentally.

I. INTRODUCTION

Human locomotion gaits consist of multiple instances of both single and double support phases (or domains),[1] with switching between these phases occurring as a result of changes in contact points with the environment, e.g., a heel-strike and a toe-off as shown in Fig. 1.[2] The multi-domain, or multi-contact nature of the human gait results in walking that is both fluid and efficient.[3,4] Using the heel-off during the single support phase, a human can lift the swing leg higher, and thus achieve greater foot clearance without bending the swing knee significantly. With the whole body rotating around the stance toe joint, it requires much less energy for human to move forward through the beneficial utilization of rotational momentum, which, therefore, is found to be important for achieving fast walking.[5] While dealing with these foot dynamic changes is seemingly effortless for a human, it is quite challenging to incorporate these advantages into bipedal robot locomotion. Motivated by the advantages and challenges, multi-contact locomotion with foot motion has been studied actively in the recent decade aiming to achieve close human-like locomotion (a few examples can be found in[6,7,8]). In particular, the overall objective of this paper is to take the first steps toward a formal means by which multi-contact robotic walking can be formally achieved. More importantly, with the additional of a trajectory generation methodology based upon the theoretic constructions, we show that these formal results can be realized experimentally on physical robots. These results are then verified on two different bipedal robot platforms, AMBER2 and ATRIAS, which are shown in Fig. 4.

A. Relationship with Previous Results

Bipedal robotic walking has been studied from a variety of viewpoints, many of which are aimed at achieving human-like locomotion capabilities on bipedal robots, i.e., achieving the stability and robustness found in human walking. From this perspective, the role of the multi-contact foot behavior is found to be essential to the locomotion of human both in biomechanical research and from studies of human walking gait. Thence, it becomes necessary to understand and reproduce
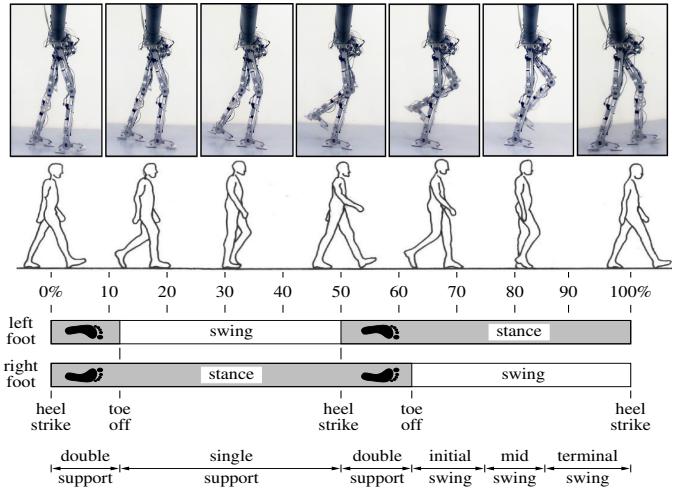

Fig. 1: Walking tiles of the multi-contact locomotion of both ATRIAS and AMBER2 (top two figures, respectively) are compared with the diagram of a typical human gait cycle.

the role of the foot on the humanoid robot to achieve human-like locomotion. In the control and robotic field, only a few of work have been devoted to the discussion of this multi-contact feature. Gait pattern generation and gait planning methods are adopted to design the foot trajectory specifically for the multi-contact foot behavior in.[9,10] An optimized walking gait with two domains is proposed in[11] for a seven-link biped. Recent works of Nishiwaki *et al.*,[12] Sellaouti *et al.*[5] and Li *et al.*[13] show that the presence of multi-contact behavior allow to perform longer strides, walk at a higher speed, and lower torque requirement. However, the vast majority of these approaches attempt to reduce the complexity of the problem through simplifying assumptions that the stance foot is flat on the ground, i.e., the foot roll only happens at the double-support phase and the trajectory is designed revolving

around the Zero Moment Point (ZMP).[14,15] Consequently, the performance of the bipedal robots are constrained by these two assumptions from utilizing the advantages of this multi-contact feature of human locomotion, for example, the toe roll at the end of single-support phase. Simulated robotic walking with significant toe roll can be found in,[7,16] in which the authors show that the walking gait with toe roll helps with the reduced torque and faster walking speed. From the authors' knowledge, noticeably lacking from existing methods from any of these perspectives is a formal way to generate multi-contact locomotion in a manner that is both formally correct as well as physically realizable.

Recent work from the coauthors has looked toward human-locomotion for inspiration for the synthesis of walking controllers with the goal to achieve human-like robotic locomotion. Point foot model with under actuation is considered in the work;[17,18] the models with one fully actuated domain, i.e., flat-foot walking, are discussed in the cases of both 2D walking[19] and 3D walking.[20] While these work is constrained to either point foot or flat foot walking, it takes the first steps forward formally generating human-like bipedal robotic walking from human data in the cases of both under- and full- actuation. Therefore, with these results in hand, this work is ready to present a formal way to achieve multi-contact robotic walking through the inspiration of human locomotion.

B. Contribution of This Paper

With the goal of exploring a general way to produce multi-contact robotic bipedal locomotion, this paper begins by noting that the multi-contact behavior (including both continuous dynamics and discrete dynamics) present in human locomotion can be represented as a hybrid system. Therefore, a hybrid system with multiple domains is constructed to describe the multi-contact robotic locomotion in a general form. Further motivated by the human locomotion data, the *extended canonical walking function* (ECWF) is utilized to serve as a low dimensional representation of the human locomotion system. This allows for the formulation of human-inspired controllers that drive outputs of the robot to outputs of the human (as represented by the ECWF) in an exponential fashion. Motivated by the fact that the multi-contact locomotion consists of discrete dynamics, i.e., impacts, a multi-domain optimization problem is proposed to generate controller parameters that yield invariant tracking even through impacts. More importantly, this optimization problem is also subject to specific physical constraints, such as torque bounds and foot scuffing prevention; therefore, the obtained parameters can be successively translated to physical robots. Finally, with the *partial hybrid zero dynamics* (PHZD) reconstruction strategy,[21] this formal result can be translated into physical robots to achieve multi-contact robotic locomotion.

Two different robot platforms are considered as examples in this paper to verify the formal results presented in this paper: AMBER2 and ATRIAS. With the specially designed artificial feet, AMBER2 is constructed with the goal to achieve human-like locomotion with multi-contact foot behavior. Therefore, human locomotion is used as the reference model to design the

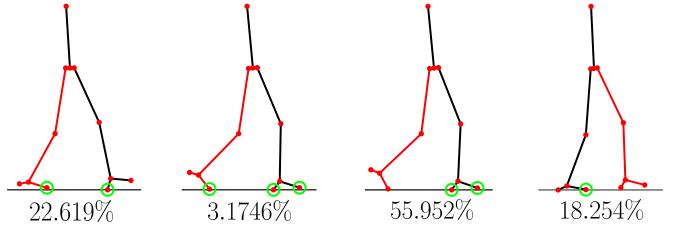22.619% 3.1746% 55.952% 18.254%

Fig. 2: Domain breakdown of one step of one subject. The numbers below each tile indicate the percentage of time spent in that domain. The green circle indicates that particular point of the foot (toe or heel) is in contact with ground. The red lines indicate the "non-stance" leg and the black lines represent the "stance" leg.

parameters of ECWF. Utilizing this reference model, human-inspired controllers are constructed through an optimization problem in order to achieve multi-domain human-like locomotion. From the perspective of achieving the main attributes of human locomotion through mechanical design, ATRIAS is designed to match key characteristics (e.g., energy efficiency) of the spring loaded invert pendulum model (SLIP), which is well-known as the low-dimensional representation of both human and animal locomotion.[22,23] To this end, the SLIP model is naturally utilized as the reference model for designing the parameters of ECWF, i.e., human-inspired controllers through a corresponding optimization problem. As a result of the formal procedure for designing multi-contact bipedal locomotion gaits, we are able to achieve both human-like multi-contact walking on AMBER2 and SLIP-like multi-contact walking on ATRIAS in both simulation and experiment.

The structure of this paper is as follows: Sec. II presents the analysis of multi-domain locomotion of both human and the low dimensional representation SLIP model. A hybrid system is developed in Sec. III to represent the multi-domain bipedal locomotion system in a general form. The constructions of the human-inspired controllers and the multi-domain optimization are explained in Sec. IV and Sec. V, respectively. In addition, both AMBER2 and ATRIAS are discussed side-by-side throughout the paper to motivate the concepts presented. Experimental realization on both AMBER2 and ATRIAS are illustrated in Sec. VI, showing that the formal results can be translated to physical robots successfully. Finally, the discussion and conclusion are presented in Sec. VII.

II. MULTI-DOMAIN LOCOMOTION

Since the results presented in this paper are inspired by human locomotion, this section carefully reviews the multi-domain aspects of the human gait—a characteristic that is intrinsic to human locomotion. Based upon experimental human data and the corresponding kinematics, three domains are extracted and utilized to characterize one step cycle of human walking. To demonstrate that these observations can be applied beyond the human locomotion, we also explore SLIP-like locomotion and its corresponding multi-domain behavior. In particular, two domains of single/double support phases are considered for the multi-domain SLIP-like locomotion considered in this paper.
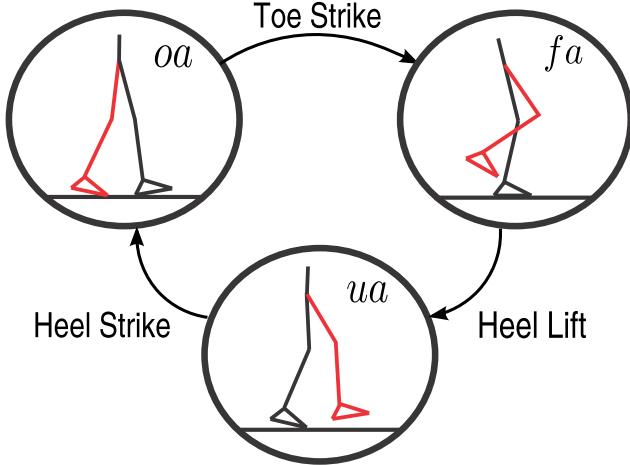
Fig. 3: The three domains represent the predominant discrete domains present in human locomotion over the a step course.

Fig. 4: Bipedal robots AMBER2 (left) and ATRIAS (right).

A. Multi-Domain Structure of Human Walking

Understanding the walking pattern of a normal leg is of obvious importance when attempting to reproduce it in robots. A human walking gait nominally consists of two phases: stance phase, when the foot is on the ground, and swing phase, when the foot is in the air.[24] Sub-phases are usually extracted from each phase to describe human locomotion more explicitly. At the highest level, we divide the walking gait into two phases consisting of a single support phase in which only one foot is in contact with the ground and double support in which both feet are in contact with the walking surface as depicted in Fig. 1.[2] Though different approaches have been applied to break one step into different phases (for example, in impedance prosthetic control,[25] the single support phase is divided into two sub-phases based on the flexion and extension of the swing knee angle), this paper breaks each step into different distinct phases based upon the points on the feet that are in contact with the ground.

Locomotion Domain Breakdown. With the goal of utilizing human data to construct robotic walking gaits, we consider the human locomotion data obtained through a high speed motion capture system (details can be found in[18]). Using the domain breakdown strategy discussed in,[18] one step is divided into four sub-phases with specific contact point configurations as shown in Fig. 2. In particular, one can note that there is one sub-phase that only takes 3.1746% of one step, to be more specific, the phase in which the front foot is flat and the back foot has only the toe in contact with the walking surface. Due to its short duration, omission of this phase simplifies control construction but without sacrificing the essential domain structure present in human locomotion. Therefore, this work will focus on the other three domains of a single step as shown in Fig. 3.

Example 1. AMBER2 (**A** & **M** **B**ipedal **E**xperimental **R**obot), a 2D footed bipedal robot with seven links, was custom built by the authors (in collaboration with the rest of AMBER Lab) with the specific goal of multi-contact locomotion as indicated by the novel design of the feet(as shown in Fig. 4). The
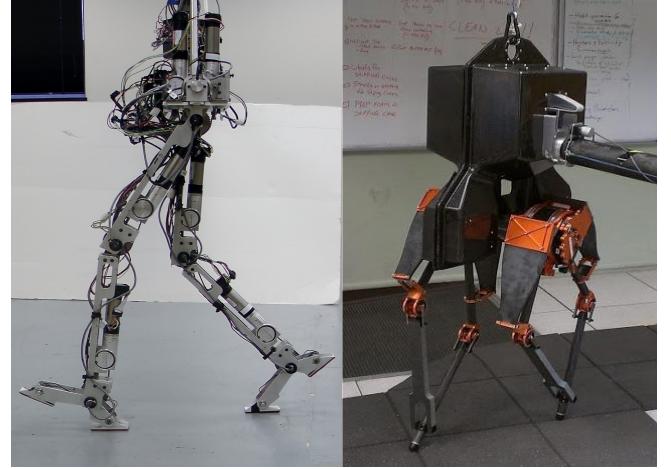
six joints of AMBER2 are actuated by brushless DC motors. Therefore, when the robot stands on the stance toe only, there is one degree of freedom that is not actuated. As a planar robot, the motion of AMBER2 has been restricted to the sagittal plane via a boom, which is configured as a parallel four-bar link mechanism such that no support in the sagittal plan is provided by the boom.[19] The boom is fixed rigidly to a low friction rotating mechanism, which allows the biped to walk in a circular fashion. In addition, counterweights are provided to negate the weight of the boom on the robot; importantly, the weight of the robot is not supported by the boom.

B. Multi-Domain of SLIP Model

The Spring Loaded Inverted Pendulum (SLIP) model provides a low-dimensional representation of locomotion by utilizing an energy-conserving spring mass model. As such, it can provide an approach for generating efficient gaits on bipedal robots.[26,27,28,29] The spring-mass model consists of a point mass m supported by two massless linear spring legs with fixed rest length r_0 and stiffness k. The spring forces only act on the mass while in contact with the ground and cannot apply forces during swing. Letting p_{com} be the position of the point mass with respect to a fixed origin, the dynamics of the SLIP model is given as follows:

$$\ddot{p}_{com} = \frac{1}{m}\left(F_R(p_{com}) + F_L(p_{com})\right) - g_e, \qquad (1)$$

where F_R and F_L are the spring forces of the legs and g_e is the gravitational vector.

The SLIP walking model consists of two different dynamical phases: single support and double support, identified by the contact constraints of the system. A stable walking gait can be obtained by selecting a proper "touch down" angle, α_{TD}, as shown in Fig. 5. Since the legs are assumed to be massless and the only control input (touchdown angle) does not require any net actuator work, the system conserves energy.

In this paper, we use model parameters that roughly approximate the low-dimensional dynamics of ATRIAS. Stable walking gaits for the given parameters are generated by
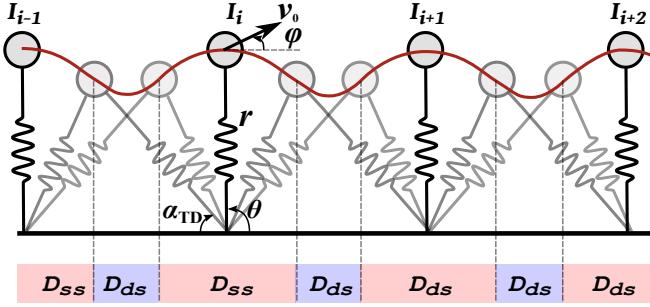
Fig. 5: The Spring Loaded Inverted Pendulum Walking Gait.

utilizing the method introduced in,[29] and the desired "touch down" angles are determined correspondingly.

Example 2. ATRIAS (**A**ssume **T**he **R**obot **I**s **A S**phere), as shown in Fig. 4, is a 3D capable, human-scale, bipedal robot conceived and implemented at the Oregon State University Dynamic Robotics Laboratory. Designed to match key characteristics of the SLIP model, ATRIAS uses large springs in series with actuators to drive lightweight four-bar mechanisms on each leg which terminates in point foot. This enables ATRIAS to achieve agile, efficient and highly dynamic maneuvers. Two brushless DC motors for each leg are mounted at the hip joint to match the SLIP model feature of concentration of robot mass. These motors drive the upper two members of the four-bar leg through a large series spring. For the current work, a support boom is used to constrain torso rotation and translation to the sagittal plane, effectively planarizing the dynamics (detailed description of the robot is presented in[30]).

III. MULTI-DOMAIN HYBRID SYSTEM

By considering the changes in contact points over a gait cycle, this section presents a hybrid system model, consisting of both continuous and discrete dynamics, as the mathematical means to capture the essential dynamics of multi-domain locomotion. To make the discussion explicit, the hybrid systems representing the two robots: AMBER2 and ATRIAS are developed side-by-side.

A. Hybrid System Model

Multi-domain robotic locomotion can be formally modeled as a hybrid control system,[31,32] which is given by the following tuple:

$$\mathscr{HC} = (\Gamma, D, S, \Delta, FG), \tag{2}$$

where

- $\Gamma = (V, E)$ is a *directed circle* graph, with vertices $V = \{v_1, v_2, ..., v_N\}$; and edges $E = \{e_1, e_2, ..., e_N\}$, where N is the number of the total domains. e_i denotes the transition from the source domain $sor(e_i)$ to the target domain $tar(e_i)$: $v_i \to v_{i+1}$ if $i < N$ and $v_N \to v_1$ if $i = N$.
- $D = \{D_v\}_{v \in V}$ is a set of *domains of admissibility*, where $D_v \subseteq X \times U$ with $X \subseteq \mathbb{R}^{2n}$ the state space set and $U \subseteq \mathbb{R}^{m_r}$ the set of admissible controls,
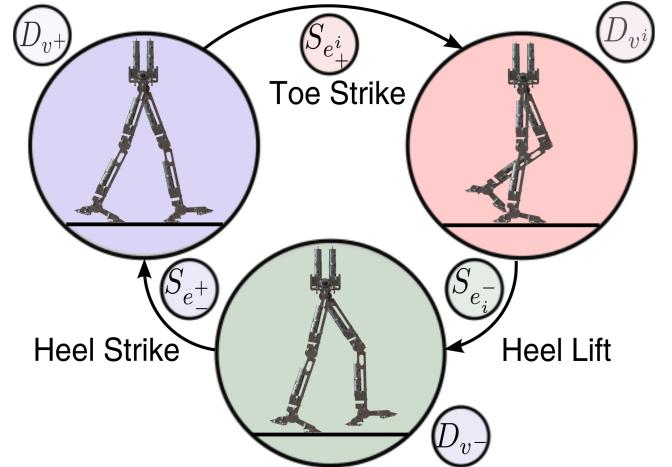

Fig. 6: The directed graph of 3 domain walking.

- $S = \{S_e\}_{e \in E}$ is a set of *guards* with $S_e \subseteq D_{tar(e)}$,
- $\Delta = \{\Delta_e\}_{e \in E}$ is a set of *reset maps*, where $\Delta_e : X \to X$ is a smooth map,
- $FG = \{(f_v, g_v)\}_{v \in V}$ with (f_v, g_v) a *control system* on D_v, i.e., $\dot{x} = f_v(x) + g_v(x)u$ with $x \in X$, $u \in U$ and $\{x, u\} \in D_v$.

Correspondingly, a *hybrid system* is a hybrid control system with $U = \emptyset$, e.g., after any feedback controllers have been applied, making the system closed-loop. In this case,

$$\mathscr{H} = (\Gamma, D^X, S^X, \Delta, F^X), \tag{3}$$

where $D^X = \{D_v^X\}_{v \in V}$ is the set of domains with $D_v^X \subset X$ being a smooth subset of only X. Similarly, $S^X = \{S_e^X\}_{e \in E}$ is the set of guards with $S_e^X \subseteq D_{tar(e)}^X$, and $F^X = \{f_v^X\}_{v \in V}$ is a set of *dynamical systems* on X, i.e., $\dot{x} = f_v^X(x)$ with $x \in D_v^X$.

Remark 1. Motivated by the desire to be able to discuss the multi-contact locomotion in the context of hybrid system in a general fashion, we label the domains explicitly based on the major impact[1] in this work. Therefore, for the multi-domain walking gait of interest (with number of domains less or equal than 3, i.e., $N \leq 3$), the vertices of the directed graph Γ are specifically defined as:

$$V = \{v^+, v^i, v^-\}, \tag{4}$$

where $+$, i and $-$ represent post-impact, intermediate and pre-impact, respectively. The edges are defined to be the transitions of interest. For example, edge e_+^i denotes the transition from the post-impact domain to the intermediate domain. For multi-domain locomotion with only two domains, the intermediate domain will be dropped for simplicity of notation. In particular, the directed graph Γ for multi-domain locomotion will always start with v^+ and end with v^-. Note

---

[1]It is possible that for a particular multi-domain hybrid system, there may be more than one impact. However, it is often the case that certain impact may be considered "soft" impact, thus not imparting a large impulse to the system. Toe strike for example could be considered a soft impact since the toe does not generally impact the ground with a considerable velocity. Heel strike, however, can have a large effect on the system and is not generally ignored. Therefore, it is considered the major impact.
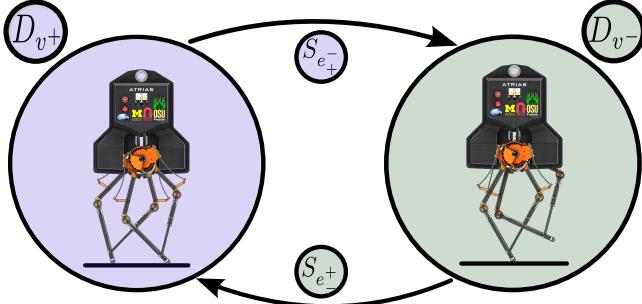
Fig. 7: The directed graph of single/double support domain.

Fig. 8: Coordinates of AMBER2 (left) and ATRIAS (right).

that assuming that the number of domains is less than or equal to 3 is a reasonable assumption for bipedal locomotion for most cases (especially given the analysis of human locomotion data given in Sect. II). That being said, the work presented in this paper is applicable to walking with any number of discrete domains through straightforward extensions.

Example 3. For the multi-domain locomotion of AMBER2, the hybrid control system can be defined as:

$$\mathscr{HC}_R = (\Gamma_R, D_R, S_R, \Delta_R, FG_R), \tag{5}$$

where the subscript R comes from the last letter of AMBER. The corresponding hybrid system can be defined as:

$$\mathscr{H}_R = (\Gamma_R, D_R^X, S_R^X, \Delta_R, F_R^X). \tag{6}$$

As motivated by the discrete domains found in human locomotion (as discussed in Ex. 1), the directed graph Γ_R with three vertices and edges will be considered as follows:

$$V_R = \{v^+, v^i, v^-\}, \tag{7}$$
$$E_R = \{e_+^i = (v^+ \to v^i), e_i^- = (v^i \to v^-), e_-^+ = (v^- \to v^+)\}.$$

The corresponding discrete domain structure for AMBER2 is shown in Fig. 6. Additionally, the major impact happens when the swing heel strikes the ground.

Example 4. In a manner analogous to AMBER2, the hybrid control system of the multi-domain locomotion of ATRIAS will be defined to be:

$$\mathscr{HC}_S = (\Gamma_S, D_S, S_S, \Delta_S, FG_S), \tag{8}$$

where the subscript comes from the last letter of ATRIAS. The corresponding hybrid system can be defined as:

$$\mathscr{H}_S = (\Gamma_S, D_S^X, S_S^X, \Delta_S, F_S^X). \tag{9}$$

Due to the fact that ATRIAS has point feet, two discrete domains are considered: single and double support. As a result, the vertices and edges of the directed graph, as shown in Fig. 7, are defined to be:

$$V_S = \{v^+, v^-\},$$
$$E_S = \{e_+^- = (v^+ \to v^-), e_-^+ = (v^- \to v^+)\}. \tag{10}$$

In particular, double support is considered as post-impact domain and single support is defined as pre-impact domain. Toe strike, the only impact, is thus the major impact of the SLIP-like multi-domain hybrid system.
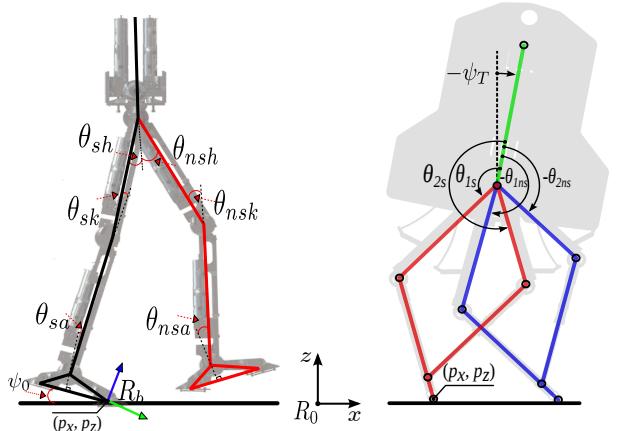
B. Coordinates, Constraints and Actuation Types

To explicitly construct the hybrid system corresponding to multi-domain locomotion, the basic concepts related to coordinates, constraints and actuation types are introduced in a general form.

Coordinates. Due to the changes of contact points between the robot and the walking surface throughout the course of a gait, generalized coordinates for the unpinned model are utilized. Specifically, for a planar robot, the configuration space $Q = \mathbb{R}^2 \times SO(2) \times Q_b$ is represented in the generalized coordinates as $\theta = \{\theta_e, \theta_b\}^T$ with the extended coordinates $\theta_e = \{p_x, p_z, \varphi_0\}$ representing the positions and rotation angle of the body fixed frame R_b with respect to a fixed inertial frame R_0; and θ_b denoting the body coordinates, which are the relative joint angles of the robot. With n denoting the general degrees of freedom of the unconstrained robot, the state space of the model is denoted accordingly as $X := \{x = (\theta; \dot{\theta}) | \theta \in Q, \dot{\theta} \in \mathbb{R}^n\}$.

Contact Conditions. With a given vertex $v \in V$, the domain D_v, which describes the admissible configuration of the system, is restricted by the constraints associated with specific contact points interacting with the walking surface. In particular, holonomic constraints, denoted as ι_v, are used to ensure that the points on the robot in contact with the ground remain in contact. Alternatively, unilateral constraints, denoted by h_v, points on the robot that can impact the ground or are used to calculate reaction forces at points that can lift from the ground.

Actuation Types. With the notions of coordinates and constraints, we can explicitly define full, over and under actuation. Let m_r denote the number of actuators on the robot—therefore, the general control set can be taken as $U = \{u | u \in \mathbb{R}^{m_r}\}$—and n_{ι_v} represent the number of holonomic constraints, we say that a domain is,

- *Fully-actuated (fa)*, if $m_r = n - n_{\iota_v}$,
- *Under-actuated (ua)*, if $m_r < n - n_{\iota_v}$,
- *Over-actuated (oa)*, if $m_r > n - n_{\iota_v}$.

Note that these actuation types can characterize all the types of actuation present in locomotion, i.e., $\forall v \in V, v \in \{\text{fa}, \text{ua}, \text{oa}\}$.

Example 5. For the coordinates of the planar robot AMBER2, the body fixed frame is located at the position of the stance toe. Therefore, $\{p_x, p_z\}$ denote the x and z positions of the stance toe w.r.t the ground frame, respectively; φ_0 is the pitch angle measured from the walking surface to the foot; and $\theta_b = \{\theta_{sa}, \theta_{sk}, \theta_{sh}, \theta_{nsh}, \theta_{nsk}, \theta_{nsa}\}$ as shown in Fig. 8. In the context of the multi-domain walking gait of interest, the constraints and actuation types of each domain of AMBER2 can be defined explicitly as shown in Fig. 3, the details of which are omitted here and can be found in.[21]

Example 6. The generalized coordinates of ATRIAS are defined as follows: with the body fixed frame being located at the terminal of the stance foot, the extended coordinates are denoted by the position term $\{p_x, p_z\}$ and the body pitch angle φ_T as $\theta_e = \{p_x, p_z, \varphi_T\}$. The coordinates of rigid part of the robot, $\theta_b = \{\theta_{1s}, \theta_{2s}, \theta_{1ns}, \theta_{2ns}\}$, and the corresponding motor coordinates, $\theta_m = \{\theta_{m1s}, \theta_{m2s}, \theta_{m1ns}, \theta_{m2ns}\}$, together form the body coordinates of the model, as shown in Fig. 8. Therefore the configuration space Q is given in the generalized coordinates as:[26]

$$\theta = \{\theta_e, \theta_b, \theta_m\}^T. \tag{11}$$

Note that, due to the existence of the series compliance, the sum of the number of actuators and the constrained degrees of freedom is always smaller than the general degrees of freedom n. That is, the robot is always under-actuated during both domains. The constraints for each domain of ATRIAS, therefore can be defined explicitly, which can be found in.[26]

C. Robot Dynamics

With the generalized coordinates and contact constraints in hand, we now construct the continuous control system FG for each domain D_v of the hybrid control system $\mathscr{HC}$.

Continuous Dynamics. Given the mass and inertia properties of each link of a specific robot (typically obtained via a CAD model or system identification method), the continuous dynamics can be constructed using the Euler-Lagrangian equations.[33] Holonomic constraints are then added to enforce the contact conditions (additional details can be found in[34]). The end result is a constrained dynamical system:

$$M(\theta)\ddot{\theta} + H(\theta, \dot{\theta}) = B_v u + J_v(\theta)^T F_v(\theta, \dot{\theta}, u), \tag{12}$$

$$J_v(\theta)\ddot{\theta} + \dot{J}_v(\theta)\dot{\theta} = \mathbf{0}, \tag{13}$$

where $M(\theta) \in \mathbb{R}^{n \times n}$ is the inertial matrix, and $H(\theta, \dot{\theta}) = C(\theta, \dot{\theta})\dot{\theta} + G(\theta) \in \mathbb{R}^{n \times 1}$ contains the terms resulting from the centripetal Coriolis effect $C(\theta, \dot{\theta})\dot{\theta}$ and the gravity term $G(\theta)$. $B_v \in \mathbb{R}^{n \times m_r}$ denotes the torque distribution matrix and $u \in U$ is the input torque vector. $F_v(\theta, \dot{\theta}, u)$ is a vector containing a contact wrench for each point on the robot in contact with the walking surface and $J_v(\theta)$ is the corresponding *Jacobian* matrix of the holonomic constraints, i.e., the contact points of a particular domain. To be more specific, the elements of the Jacobian matrix are the first-order partial derivatives of the generalized position vector (including both the translational position and the planar rotation) of the contact points in that domain v. F_v can be explicitly derived from the states x and

the controller u by substituting the holonomic constraints as shown in (13) into (12), which yields:

$$F_v(\theta, \dot{\theta}, u) = - (J_v(\theta)M(\theta)^{-1}J_v(\theta)^T)^{-1}(\dot{J}_v(\theta, \dot{\theta})\dot{\theta} + \tag{14}$$
$$J_v(\theta)M(\theta)^{-1}(B_v u - H(\theta, \dot{\theta}))).$$

The detailed derivation is omitted here and can be found in.[33]

Converting the equations of motion to a first order ODE yields the affine control system (f_v, g_v), which can be written in coordinates in the following form: $\dot{x} = f_v(x) + g_v(x)u$ (see[35] for details).

Discrete Dynamics. Due to the presence of impacts and the varying nature of the contact points throughout a gait cycle, we have to carefully consider the modeling of domains D_v, guards S_e, and reset maps Δ_e, for a hybrid system given in (2). These elements of a multi-domain hybrid system model will be explicitly constructed using the unilateral and holonomic constraints as defined above.

Given a vertex $v \in V$, the continuous domain is the set of admissible configurations of the system factoring in both normal reaction forces and a unilateral constraint. Specifically, from the wrench $F_v(\theta, \dot{\theta}, u)$, one can ensure that the foot is both in contact with the ground and no slipping by considering inequalities in the form: $R_v^T F_v(\theta, \dot{\theta}, u) \geq 0$ with R_v^T defined as coefficients of the normal reaction forces and the static friction conditions for domain D_v. For example, with only one contact point, R^T can be defined as $[0, 1; -1, \mu]$, where μ is the static friction coefficient (see[36] for more details). These are coupled with the unilateral constraint on this domain, $h_v(\theta, \dot{\theta}, u)$, yielding the set of admissible configurations:

$$\mathcal{A}_v(\theta, \dot{\theta}, u) = \left[\begin{array}{c} R_v^T F_v(\theta, \dot{\theta}, u) \\ h_v(\theta, \dot{\theta}, u) \end{array} \right] \geq \mathbf{0}. \tag{15}$$

With this setup, the domains and guards are thus given as:

$$D_v = \{(\theta, \dot{\theta}, u) \in X \times U : \mathcal{A}_v(\theta, \dot{\theta}, u) \geq \mathbf{0}\}, \tag{16}$$

$$S_e = \{(\theta, \dot{\theta}, u) \in X \times U : h_v = 0 \text{ and } \dot{h}_v < 0\}. \tag{17}$$

In particular, the guard is the boundary of this domain with the additional condition that the unilateral constraint is decreasing.

The impact equations are given by considering the holonomic constraints enforced on the subsequent domain. In particular, the post-impact velocity $\dot{\theta}^+$ is given in terms of the pre-impact velocity $\dot{\theta}^-$. Note that as a result of considering "stance" and "non-stance" legs, the labeling on the legs must be switched during one of the transitions, which occurs at major impact. This is a common "trick" in robotic walking used to reduce the number of discrete domains. With this, the reset map is given by,

$$\Delta_e(\theta, \dot{\theta}) = \left[\begin{array}{c} \Delta_{\theta, e}\theta \\ \Delta_{\dot{\theta}, e}(\theta)\dot{\theta} \end{array} \right]. \tag{18}$$

To be more explicit, $\Delta_{\theta, e} = \Delta_{\dot{\theta}, e}(\theta) = I_{n \times n}$ for the smooth transitions, i.e., transitions without relabeling or impact. For the transition with impact which is also the moment when the relabeling should be considered, $\Delta_{\theta, e}$ is the relabeling matrix and $\Delta_{\dot{\theta}, e}(\theta)$ is impact reset map. Note that, the impact reset map is computed assuming perfectly plastic (i.e., inelastic)

impacts, which is a common practice in the bipedal research literature.[16,34,46] In particular, the velocity of the swing foot is assumed to be zero (no rebound or slipping) after impacts and there is no instantaneous change in the configuration.[45]

Example 7. With the coordinates and constraints of AMBER2 defined in Ex. 5, the continuous dynamics, domains D_v, guards S_e and reset maps Δ_e for AMBER2 can be configured explicitly according to the discussion above. Note that, in order to capture the actual behavior of the physical system, the mathematical model of AMBER2 also contains the inertial modeling of the motors and the boom; the detailed derivation can be found in.[21]

Example 8. For ATRIAS, the domains D_v, guards S_e and reset maps Δ_e can be configured correspondingly with the framework discussed above. Considering the existence of spring dynamics in ATRIAS, the control system (f_v, g_v) can be obtained from the Lagrangian dynamics of a n-DOF robot with series compliant actuators:[38]

$$D(\theta_z)\ddot{\theta}_z + H(\theta_z, \dot{\theta}_z) - B_{sp}\tau_{sp}(\theta_b, \theta_m, \dot{\theta}_b, \dot{\theta}_m) = J_v(\theta_z)^T F_v, \quad (19)$$

$$J_m\ddot{\theta}_m + \tau_{sp}(\theta_b, \theta_m, \dot{\theta}_b, \dot{\theta}_m) = B_m u, \quad (20)$$

$$J_v(\theta_z)\ddot{\theta}_z + \dot{J}_v(\theta_z)\dot{\theta}_z = \mathbf{0}, \quad (21)$$

where $\theta_z = \{\theta_e, \theta_b\}^T$ is the coordinates of the rigid body system without series springs, $D(\theta_z)$ and $H(\theta_z, \dot{\theta}_z)$ are the inertial matrix and the sum of the Coriolis effect and the gravity vector of the rigid body dynamics, J_m is the motor inertia, $u \in U_S$ is the control input of motors, $B_m \in \mathbb{R}^{4 \times 4}$ is the motor torques distribution matrix, $J_v(\theta_z)$ is the Jacobian of the holonomic constraints defined for each domain and F_v is the vector of reaction forces acting on the contact point that can be computed in terms of state variables and control inputs.[34]. Also, $B_{sp} \in \mathbb{R}^{7 \times 4}$ is the spring force distribution matrix, and $\tau_{sp}(\theta_b, \theta_m, \dot{\theta}_b, \dot{\theta}_m)$ is the vector of spring forces. The detailed derivation of the control system for each domain $\{f_v, g_v\}$ has been shown in the author's previous work.[26]

IV. HUMAN-INSPIRED CONTROLLER

This section extends the traditional framework of the human-inspired control in[31,35] to the multi-contact case. The canonical walking function is proposed to characterize the multi-domain locomotion in a unified form, based on which, a human-inspired controller is constructed explicitly for the automatic generation of multi-domain walking gaits.

A. Control Output of Locomotion System

Consider the continuous system with the specific outputs defined on each domain D_v as given by:

$$\dot{x} = f_v(x) + g_v(x)u,$$
$$y_v = y_v^a(x) - y_v^d(x), \quad (22)$$

with y_v the *control outputs* for $v \in V$, consisting of the differences between the actual outputs, $y_v^a(x)$, and the desired value for these outputs, $y_v^d(x)$. The human-inspired control design process consists of determining the proper choice of actual and desired outputs, along with the construction of a control law u that drives $y_v^a(x) \to y_v^d(x)$ such that the resulting hybrid system obtained by applying this control law has a periodic orbit, i.e., a stable walking gait.

B. Human Locomotion Outputs

Motivated by the goal of achieving human-like robotic walking,[24] the actual human outputs are extracted from the human locomotion data to represent the locomotion patterns of a human throughout a step with the goal of control synthesis. In particular, we formally define a human output combination as follows:[31]

Definition 1. *A human output combination for $v \in V$ is a tuple $Y_v^H = (Q, y_{1,v}^H, y_{2,v}^H)$ consisting of a configuration space Q, velocity-modulating outputs $y_{1,v}^H : Q \to \mathbb{R}^{n_{1,v}}$ and position-modulating outputs $y_{2,v}^H : Q \to \mathbb{R}^{m_v - n_{1,v}}$ with $n_{1,v}$ the number of velocity-modulating outputs and m_v the available degrees of actuation. Specifically, $n_{1,v} = 1$ for $v \in \{V_{\mathrm{fa}}, V_{\mathrm{oa}}\}$ and $n_{1,v} = 0$ for $v \in V_{\mathrm{ua}}$. Let O_v be an index set for $y_{2,v}^H$ whereby $y_{2,v}^H(\theta) = [y_{2,v}^H(\theta)_o]_{o \in O_v}$.*

A human output combination is *independent* if

$$rank\left(\begin{bmatrix} y_{1,v}^H(\theta) \\ y_{2,v}^H(\theta) \end{bmatrix}\right) = m_v, \quad (23)$$

on Q_b; and linear if

$$y_{1,v}^H(\theta) = c_v\theta, \quad (24)$$
$$y_{2,v}^H(\theta) = H_v\theta, \quad (25)$$

for $c_v \in \mathbb{R}^{n_{1,v} \times n}$ and $H_v \in \mathbb{R}^{(m_v - n_{1,v}) \times n}$. Note that this definition is not limited to the human locomotion data, but can also be applied to different types of reference output data, e.g., one can consider a SLIP model output combination. The following two examples illustrate the outputs selection of both the human-like model AMBER2 and the SLIP-like model ATRIAS.

Example 9. Investigation of human locomotion data reveals that seven linear independent outputs can be chosen as candidates to characterize the human-like model of AMBER2:[21] $\delta p_{hip}(\theta)$, the linearized forward position of the hip measured from the stance ankle joint; θ_{sa}, the stance ankle angle; θ_{sk}, the stance knee angle; θ_{nsk}, the non-stance knee angle; θ_{hip}, the hip angle between two thighs; $\theta_{tor}(\theta)$, the torso angle measured from the vertical, and $\theta_{nsf}(\theta)$, the angle of the non-stance foot w.r.t the horizontal. Additional details, along with these outputs as calculated from experimental human walking data, can be found in.[18,31]

Specifically, the linearized hip position is utilized as the velocity-modulating output and is characterized by c_v. Since the pre-impact domain $v^- \in V_{\mathrm{ua}}$, only the post-impact and intermediate domain have the velocity-modulating output. The remaining six position-modulating outputs can be written in the matrix form H_{v^-}. Note that, the explicit expressions of c_v and H_{v^-} of AMBER2 are omitted here for simplicity and can be found in.[21] The motivation for using the notation H_{v^-} is that the position-modulating output combination is also the output combination for the pre-impact (under-actuated)

domain for AMBER2. The position-modulating outputs for the post-impact and intermediate domains are chosen to be sub-matrices of H_{v-} based upon the available degrees of actuation in each of these domains. In particular, $H_{v+} = (H_{v-})_{1,2,5,6}$ and $H_{v^i} = (H_{v-})_{2-6}$, where we use the notation $(H_{v-})_i$ to denote the ith row of H_{v-}.

Example 10. As discussed in Sec. II-B for ATRIAS, the center of mass trajectories are the natural choice for representing the reduced order SLIP model. However, for the full-order robotic system, the complex nonlinear expression for the center of mass position will significantly increase the complexity of the controller. Therefore, we instead consider a linear combination of state variables that approximately characterize the simple SLIP model dynamics. In particular, the following collection of outputs, first proposed in Eq. (14) of,[39] yields such a representation:

- Virtual stance leg angle: $\theta_{sl} := \left(\frac{\theta_{m2s}+\theta_{m1s}}{2}\right)$,
- Virtual non-stance leg angle: $\theta_{nsl} := \left(\frac{\theta_{m2ns}+\theta_{m1ns}}{2}\right)$,
- Angle of the stance knee: $\theta_{sk} := (\theta_{m2s} - \theta_{m1s})$,
- Non-stance knee angle: $\theta_{nsk} := (\theta_{m2ns} - \theta_{m1ns})$,

where the virtual leg angles characterize the forward motion of the legs and the knee angles determine the corresponding leg lengths. Note that we use motor angles instead of joint angles due to the following considerations: (1) motor angles are directly controlled, therefore we can track them more precisely, and (2) assuming small spring deflections, motor angles are good approximations of the joint angles in the context of calculating center of mass position. This observation will facilitate the construction of the gait generation optimization problem utilizing the SLIP model as a reference.

With the motivation to formalize the output combination according to Def. 1, the linearized hip position (defined as c_v) is chosen as the velocity-modulating output for both domains and used as the parameterization of time for the feedback controller. Due to the presence of elasticity in ATRIAS, the robot is under-actuated in both *single support* and *double support* domain. Hence, in contrast to the constructions for AMBER2, we define the same combination of position-modulating outputs for both single and double domains of ATRIAS. Those outputs can be characterized by the matrix H_v followed by the previous definition of outputs. The detailed expression of c_v and H_v for ATRIAS is omitted here and can be found in.[26] The end result is a set of outputs for which the corresponding feedback control law is implemented via the human-inspired controller that will be introduced in Sec. IV-D.

C. Robotic Human-Inspired Outputs

With the actual human locomotion outputs in hand, the next step is to search for specific walking functions to characterize the behavior of the human locomotion, while with the hope that the fundamental mechanisms underlying human walking can be discovered, simplified and exploited to achieve robust walking in bipedal robots.

Extended Canonical Walking Function. Previous work reveal that the actual human outputs considered for various types of locomotion (flat-ground walking[35] and running[40])

can be characterized by a simple function characterizing the solution to a linear spring-mass-damper system, which we termed the *canonical walking function* (CWF). That is, the human locomotion system appears to display simple behavior when locomoting in a periodic fashion. In addition, studying human locomotion data for more complex locomotion types, e.g., stair climbing[41] and rough terrain walking,[18] the actual human outputs can be characterized by a natural extension to the canonical walking function consisting of a linear mass-spring-damper system subject to sinusoidal excitation. Further justification of these concepts can be found in.[18]

In this work, it is found that the actual multi-domain human locomotion outputs for a complete step cycle can be characterized by this extended function, which we term the *extended canonical walking function* (ECWF):

$$y_{ecwf}(t) = e^{-\alpha_4 t}(\alpha_1 \cos(\alpha_2 t) + \alpha_3 \sin(\alpha_2 t)) + ... \\ \alpha_5 \cos(\alpha_6 t) + \kappa(\alpha)\sin(\alpha_6 t) + \alpha_7, \quad (26)$$

where $\kappa(\alpha) = (2\alpha_4\alpha_5\alpha_6/((\alpha_2)^2+(\alpha_4)^2+(\alpha_6)^2))$. Analysis of the chosen position-modulating human outputs shows that this function can fit the human locomotion data with high correlation, i.e., multi-domain human locomotion can be accurately represented by this simple function.

Parameterization of Time. Noted for the study of the selected human outputs, the linearized forward hip position can be approximated by a linear function of time $\delta p_{hip}(t) = \text{v}_{hip}t$ throughout a single step; therefore, this is chosen to be the desired behavior for the velocity modulating output. Through this observation, and with the goal of controlling the velocity of the robot, we define the following relative degree one output:

$$y_{1,v}^a(\theta,\dot{\theta}) = \dot{y}_{1,v}^H(\theta,\dot{\theta}) = dy_{1,v}^H(\theta)\dot{\theta}, \quad y_{1,v}^d(\alpha) = \text{v}_{hip}. \quad (27)$$

To define the actual and desired outputs for the position modulating outputs, we begin by noting that—due to the linearity of the hip velocity —we can parameterize time in the following fashion:

$$\tau(\theta) = (\delta p_{hip}(\theta) - \delta p_{hip}(\theta^+))/\text{v}_{hip}, \quad (28)$$

which removes the dependence of time in (26) and renders an autonomous ECWF that only depends on the states.[37] Note that, θ^+ represents the robot configuration at the beginning of one step. Therefore, the desired outputs y_2^d can be stated as:

$$y_{2,v}^d(\tau(\theta),\alpha_v) := [y_{ecwf}(\tau(\theta),\alpha_v)_o]_{o \in O_v}. \quad (29)$$

Correspondingly, the actual outputs can be obtained through the position-modulating outputs as:

$$y_{2,v}^a = y_{2,v}^H(\theta) = H_v\theta. \quad (30)$$

Robotic Human-Inspired Outputs. With the autonomous ECWF in hand, we formally define the robotic human-inspired outputs for the robot as:

$$y_v(\theta,\dot{\theta},\alpha_v) = \begin{bmatrix} y_{1,v}(\theta,\dot{\theta},\alpha_v) \\ y_{2,v}(\theta,\alpha_v) \end{bmatrix} = \begin{bmatrix} y_{1,v}^a(\theta,\dot{\theta}) - y_{1,v}^d(\alpha_v) \\ y_{2,v}^a(\theta) - y_{2,v}^d(\tau(\theta),\alpha_v) \end{bmatrix}, \quad (31)$$

where $y_{1,v}(\theta,\dot{\theta},\alpha_v)$ and $y_{2,v}(\theta,\alpha_v)$ are the relative degree one

and relative degree two outputs, respectively.

The parameter set α is the grouped parameters of all the outputs consisting of both the relative degree one output and relative degree two outputs for a complete step cycle. Particularly, based on the actuation type in each domain v, the corresponding components α_v of α will be utilized to define the human-inspired outputs via (26) and (27). Note that, for a specific output, the parameters will be kept unchanged for all the domains during one step cycle , i.e., only one set of parameters α is used to characterize an entire step.

D. Control Law Construction

The goal of the controller is to drive the outputs of robot to the outputs of human (or other reference trajectories of interest, e.g., SLIP-based trajectories) as represented by the ECWF in each domain. Due to the fact that the dynamics of robotic systems are highly nonlinear, input/output linearization is a natural choice of control methodology to drive $y_{\alpha_v,v} \to 0$ in an exponential fashion. In particular, in the domains of full- and over- actuation, we define the controller as:

$$u_v^\varepsilon(\theta, \dot{\theta}, \alpha_v) = -A_v^{-1}(\theta, \dot{\theta}, \alpha_v) \left(\begin{bmatrix} 0 \\ L_{f_v}^2 y_{2,v}(\theta, \dot{\theta}, \alpha_v) \end{bmatrix} \right.$$
$$\left. + \begin{bmatrix} L_{f_v} y_{1,v}(\theta, \dot{\theta}, \alpha_v) \\ 2\varepsilon L_{f_v} y_{2,v}(\theta, \dot{\theta}, \alpha_v) \end{bmatrix} + \begin{bmatrix} \varepsilon y_{1,v}(\theta, \dot{\theta}, \alpha_v) \\ \varepsilon^2 y_{2,v}(\theta, \dot{\theta}, \alpha_v) \end{bmatrix} \right), \quad (32)$$

with $v \in \{\text{fa, oa}\}$ and L the Lie derivative.[42] Note that, $\varepsilon > 0$ is a user defined control gain that determines the convergence rate of $y_{\alpha_v,v} \to 0$. The decoupling matrix $A_v(\theta, \dot{\theta}, \alpha_v)$ is given as:

$$A_v(\theta, \dot{\theta}, \alpha_v) = \begin{bmatrix} L_{g_v} y_{1,v}(\theta, \dot{\theta}, \alpha_v) \\ L_{g_v} L_{f_v} y_{2,v}(\theta, \dot{\theta}, \alpha_v) \end{bmatrix}, \quad (33)$$

which is nonsingular because of a linear and independent output combination was chosen.

For the under-actuated domain, the controller is defined as:

$$u_{ua}^\varepsilon(\theta, \dot{\theta}, \alpha_{ua}) = -A_{ua}^{-1}(\theta, \dot{\theta}, \alpha_v) \left(L_{f_{ua}}^2 y_{2,ua}(\theta, \dot{\theta}, \alpha_v) \right.$$
$$\left. + 2\varepsilon L_{f_{ua}} y_{2,ua}(\theta, \dot{\theta}, \alpha_v) + \varepsilon^2 y_{2,ua}(\theta, \dot{\theta}, \alpha_v) \right), \quad (34)$$

with $A_{ua}(\theta, \dot{\theta}, \alpha_v) = L_{g_{ua}} L_{f_{ua}} y_{2,ua}(\theta, \dot{\theta}, \alpha_v)$.

With the feedback control laws (32) and (34) in hand, the next step is to find such a parameter set α that a hybrid periodic orbit can be obtained for the multi-domain locomotion system. Guided by this objective , an optimization problem that yields the parameter set α will be presented in the next section.

Example 11. As discussed in Ex. 9, the general position-modulating outputs (i.e., relative degree two outputs) combination is also the outputs combination for the pre-impact domain for AMBER2, therefore, we use the notation α_{v-} to represent the generalized position-modulating outputs for simplicity. With the actual human outputs chosen above, the generalized position-modulating human-inspired outputs $y_{2,v-}(\theta, \alpha_{v-}) = y_{2,v-}^a(\theta) - y_{2,v-}^d(\tau(\theta), \alpha_{v-})$ with $y_{2,v-}^a(\theta) = H_{v-}\theta$ and $y_{2,v-}^d = [y_{ecwf}(\tau(\theta), \alpha_{v-})_o]_{o \in O_{v-}}$, where $O_{v-} = \{sa, sk, nsk, hip, tor, nsf\}$.

The parameter set can be obtained as $\alpha = \{\text{v}_{hip}, \alpha_{v-}\} \in \mathbb{R}^{43}$ with $\alpha_{v-} = \{\alpha_{sa}, \alpha_{sk}, \alpha_{nsk}, \alpha_{hip}, \alpha_{tor}, \alpha_{nsf}\}$. By defining $\alpha_{v_{hip}} = \{\text{v}_{hip}, 0, 0, 0, 0, 0, 0\} \in \mathbb{R}^7$, the vector components of α can be stacked in matrix form with $\alpha \in \mathbb{R}^{7 \times 7}$. Because the actuation type in each domain is different, the parameter set matrix for specific domain will be the sub-row matrices of α. In particular, $\alpha_{v+} = \alpha([1-3, 6, 7], :)$, $\alpha_{v^i} = \alpha([1, 3-7], :)$ and $\alpha_{v-} = \alpha([2-7], :)$.

Consequently, with the human-inspired outputs defined above, the human-inspired controllers can be constructed according to (32) for the post-impact and intermediate domains and (34) for the pre-impact domain.

Example 12. For ATRIAS, we define the the relative degree two actual outputs $y_{2,v}^a(\theta) = H_v\theta$ and desired outputs $y_{2,v}^d(\tau, \alpha_v) = [y_{ecwf}(\tau(\theta), \alpha_v)_o]_{o \in O_v}$, where $O_v = \{sl, nsl, sk, nsk\}$. Importantly, because the parameters for each output are exactly the same on both single support and double support domain, i.e., $\alpha_{v+} = \alpha_{v-} = \alpha$, the corresponding controller can easily be implemented on the real robot. In particular, due to the fact that the robot is under-actuated on both domains, the controllers for the affine control system for each domain can be determined from (34) explicitly.

V. MULTI-DOMAIN OPTIMIZATION

This section will focus on developing of an optimization problem that yields the parameter set α which will result in stable multi-domain robotic locomotion. Multi-domain *partial hybrid zero dynamics* (PHZD) constraints are introduced to insure the partial zero dynamics are invariant through all the discrete transitions; the end result is a formal guarantee that there is a periodic orbit for the complete system if the partial zero dynamics have a stable limit cycle. With the objective cost function being the least squares fit of the robot outputs to the corresponding outputs computed from human locomotion data, the goal is to find the parameter set α that yields a human-like multi-domain locomotion gait with guaranteed stability while simultaneously being physically realizable.

A. Partial Hybrid Zero Dynamics

Before revealing the optimization problem that will yield stable multi-contact walking gaits, it is necessary to introduce several constructions that are fundamental to its formulation.

Zero Dynamics. For under-actuated locomotion, the goal of the human-inspired control laws is to drive the relative degree two outputs $y(\theta) \to \mathbf{0}$ exponentially. In other words, the control objective is to drive the system dynamics to a parameterized smooth surface exponentially, termed the *zero dynamic surface* $\mathbf{Z}$, which is defined as the following:

$$\mathbf{Z} = \{(\theta, \dot{\theta}) \in X : y(\theta) = \mathbf{0}, \ L_f y(\theta, \dot{\theta}) = \mathbf{0}\}. \quad (35)$$

There are several advantages of studying this reduced order (or restricted) dynamics instead of the full order dynamics. For example, with less degrees of freedom, the controller design computation time which usually involves dynamics integration, can be reduced significantly (more details in [26,37]).

In particular, we begin by considering the generalized under-actuated affine control system (22), and it assumes can be represented in the zero dynamics normal form as:[42]

$$\dot{\eta} = b(\eta, \xi) + a(\eta, \xi)u, \tag{36}$$

$$\dot{\xi} = q(\eta, \xi), \tag{37}$$

where η represent the controlled normal states and $\xi \in \mathbf{Z}$ are the uncontrolled states for the zero dynamics surface. The vector fields b, a, and q are assumed to be locally Lipschitz continuous. In addition, we assume that $b(\mathbf{0}, \xi) = \mathbf{0}$, so that the zero dynamics surface $\mathbf{Z}$ (with $y(\theta) = \eta$) defined by $\eta = \mathbf{0}$ with dynamics

$$\dot{\xi} = q(\mathbf{0}, \xi), \tag{38}$$

is invariant.[43]

Partial Hybrid Zero Dynamics. The above construction is for the general under-actuated single-domain system. Considering the multi-domain hybrid zero dynamics with full- and over- actuation domains that includes relative degree one output, enforcing this invariance through impact is a strong condition that limits the behaviors of the robots. Therefore, with a view towards the importance of the relative degree two outputs $y_{2,v}(\theta, \alpha_v)$, we consider the zero dynamics by defining $y(\theta) = y_{2,v}(\theta, \alpha_v)$, which we termed the *partial zero dynamics surface*[2]:

$$\mathbf{PZ}_{\alpha_v} = \{(\theta, \dot{\theta}) \in D_v^X : y_{2,v}(\theta, \alpha_v) = \mathbf{0}, L_{f_v} y_{2,v}(\theta, \dot{\theta}, \alpha_v) = \mathbf{0}\}. \tag{39}$$

Through the exclusion of the relative degree one output in the zero dynamics, the partial zero dynamics surface $\mathbf{PZ}_{\alpha_v}$ can be specifically designed such that it is invariant for a hybrid system with multiple domains. In other words, the goal of considering the PHZD is to find the parameter set α to ensure that the zero dynamic systems remain on the surfaces through all of the discrete transitions present in the multi-domain walking. Formally stated, the hybrid control system in (2) with the directed graph defined as in (4) and the human-inspired controller defined as in (32) and (34), has PHZD if:

$$\Delta_e(S_e \cap \mathbf{PZ}_{\alpha_{sor(e)}}) \subset \mathbf{PZ}_{\alpha_{tar(e)}}, \tag{40}$$

for each transition $e \in E$. Therefore, in the case of AMBER2 with three transitions, i.e., $e \in E_R$, three sets of PHZD constraints have to be constructed. For the case of ATRIAS with two transitions, i.e., $e \in E_S$, two sets of PHZD constraints have to be developed correspondingly. A visual representation of the geometry of these constraints for the case of AMBER2 is illustrated explicitly in Fig. 9.

Note that, the formula in (36) and (37) is explicitly defined for domains with under-actuation. For the cases of full- and over- actuation, the outputs $y_v(\theta, \dot{\theta}, \alpha_v)$ can be separated into relative degree one outputs $y_{1,v}(\theta, \dot{\theta}, \alpha_v)$ and relative degree

two outputs $y_{2,v}(\theta, \alpha_v)$. Having the relative degree two outputs converged to $\mathbf{0}$, which is defined as the partial zero dynamics surface, we could explicitly define the relative degree one output as ξ_v satisfying (37) with applying a pre-feedback controller. That is to say, because of the full control authority, we could carefully shape the dynamics of relative degree one outputs to the form of (37), which can be reasonably viewed as a "controllable" zero dynamics. A detailed example can be seen in the section of PHZD reconstruction as in (42). This discussion is important because it allows the general construction of the zero dynamics as in (36) and (37) to suit for all domains with different types of actuation, which, therefore, form the framework for later discussion.

PHZD Reconstruction. With the formal constructions in place, the goal of this section is to restate the PHZD constraints in a way that can be solved numerically in an optimization problem. This is done via the PHZD reconstruction methodology. With the assumption that the system evolves on the PHZD surface, a low dimensional representation of the system can be obtained by defining the partial hybrid zero dynamics coordinates on the domains $v \in \{oa, fa\}$:

$$
\begin{aligned}
\xi_{1,v} &= \delta p_{hip}(\theta) := c_v \theta, \\
\xi_{2,v} &= y_{1,v}^a(\theta, \dot{\theta}) := \delta \dot{p}_{hip}(\theta) := c_v \dot{\theta}.
\end{aligned} \tag{41}
$$

With this choice of zero dynamics coordinates, and due to the fact that the system is fully controllable, the dynamics of this surface can be shaped explicitly according to the control purpose. Therefore, the partial zero dynamics can be designed to evolve according to the following linear system:[20]

$$
\begin{aligned}
\dot{\xi}_{1,v} &= \xi_{2,v}, \\
\dot{\xi}_{2,v} &= -\varepsilon(\xi_{2,v} - v_{hip}).
\end{aligned} \tag{42}
$$

In addition, note that the desired position modulating outputs $y_{2,v}^d$ is a function of the parameterized time τ as shown in (28); thence, it is also a function of $\xi_{1,v}$. Therefore, utilizing $\xi_{1,v}$, $\xi_{2,v}$ and the fact that on the partial zero dynamics surface we have $y_{2,v}^H(\theta) = y_{2,v}^d(\xi_{1,v}, \alpha_v)$ and $\partial y_{2,v}^H(\theta)/\partial\theta\dot{\theta} = \partial y_{2,v}^d(\xi_{1,v}, \alpha_v)/\partial\xi_{1,v}\xi_{2,v}$, we can explicitly, and in closed form, reconstruct the full order state of the robot through the formula:

$$
\begin{aligned}
\theta_v &= \Psi(\xi_{1,v}, \alpha_v) = \begin{bmatrix} c_v \\ H_v \end{bmatrix}^{-1} \begin{pmatrix} \xi_{1,v} \\ y_{2,v}^d(\xi_{1,v}, \alpha_v) \end{pmatrix}, \\
\dot{\theta}_v &= \Phi(\xi_{1,v}, \xi_{2,v}, \alpha_v) = \begin{bmatrix} c_v \\ H_v \end{bmatrix}^{-1} \begin{pmatrix} v_{hip} \\ \frac{\partial y_{2,v}^d(\xi_{1,v}, \alpha_v)}{\partial\xi_{1,v}}\xi_{2,v} \end{pmatrix}.
\end{aligned} \tag{43}
$$

Note that, the explicit coordinates in (41) and the linear ODE in (42) for the partial hybrid zero dynamics are valid for over-[3] and fully-actuated domains only. For the under-actuated domain, numerical integration of the zero dynamics is required to obtain the zero dynamics states, which will be then utilized with (43) for the reconstruction of the full-order joint state (as outlined in[35,37]).

---

[2]Note that, the reason we term this dynamics as *partial zero dynamics* is because the real zero dynamics also includes the relative degree one outputs for the full- and over- actuation domains. For the under-actuated domain that only has relative degree two outputs, the $\mathbf{PZ}_{\alpha_v}$ surface is actually the *full zero dynamic surface*, i.e., $\mathbf{PZ}_{\alpha_{ua}} := \mathbf{Z}_{ua}$. For notation simplicity, in this work, $\mathbf{PZ}_{\alpha_v}$ is adopted for both situations.

[3]For the over-actuated domain, the PHZD reconstruction only yields directly controlled states. The rest states will be computed through geometry constraints in closed form.[21]

B. Main Results.

With the goal to formally establish stable bipedal robotic walking, we start with introducing the periodic orbits of the multi-domain hybrid systems as in (3) and the corresponding generalized *Poincaré* return maps. With $D^X = D^X_{v_1} \cup D^X_{v_2} \cdots \cup D^X_{v_N}$, a solution $\varphi(t, x_0)$ of (3) is periodic if there exists a finite $T > 0$ such that $\varphi(t + T, x_0) = \varphi(t, x_0)$ for all $t \in [t_0, \infty)$ and initial condition $x_0 \in D^X$. A set $\mathscr{O} \subset D^X$ is a periodic orbit of (3) if $\mathscr{O} = \{\varphi(t, x_0) \mid t \leq t_0\}$ for some periodic solution $\varphi(t, x_0)$. Similarly, we denote the solution of the zero dynamics $\dot{\xi} = q(\mathbf{0}, \xi)$ by $\varphi_{\mathbf{Z}}(t, \xi_0)$ with $\xi_0 \in \mathbf{Z}$. Correspondingly, the periodic orbit of the zero dynamics is denoted as $\mathscr{O}_{\mathbf{Z}} \subset \mathbf{Z}$.

The *Poincaré* return map[44] is a general mathematical tool for determining the existence and stability properties of periodic orbits for hybrid dynamical systems with impulses. Analogous to the hybrid systems with a single-domain as discussed in,[31] we can obtain the generalized *Poincaré* map for domain v_i from one switching surface to anther as $P_{v_i} : S^X_{e_{i-1}} \to S^X_{e_i}$, which is a partial function:

$$P_{v_i}(x_{v_{i-1}}) = \varphi_{v_i}(T_{I_{v_i}}(\Delta_{e_{i-1}}(x_{v_{i-1}}), \Delta_{e_{i-1}}(x_{v_{i-1}})), \quad (44)$$

where $x_{v_i} \in S^X_{e_i}$ and $T_{I_{v_i}} : S^X_{e_i} \to \mathbb{R} > 0$ is the *time-to-impact* function for domain v_i:

$$T_{I_{v_i}}(x_0) := \inf\{t \leq 0 \mid \varphi_{v_i}(t, x_0) \in S^X_{e_i}\}, \quad (45)$$
$$\text{if } \exists t \text{ such that } \varphi_{v_i}(t, x_0) \in S^X_{e_i}.$$

In particular, for system (2) with the directed circle graph defined as Γ, the *Poincaré* return map can be defined with the composition of generalized *Poincaré* maps for each domain v_i as discussed in:[34]

$$P := P_{v_N} \circ \cdots \circ P_{v_1}. \quad (46)$$

With this definition, according to the Proposition in,[34] P is also the *Poincaré* map for the hybrid system with a single domain as defined in:[31]

$$\bar{\mathscr{H}} = (\bar{D}, \bar{S}, \bar{\Delta}, \bar{f}), \quad (47)$$

with $\bar{D} = D^X_{v_1}$, $\bar{f} = f^X_{v_1}$, $\bar{S} = S^X_{e_1}$ and $\bar{\Delta} = \Delta_{e_N} \circ P_{v_N} \circ \cdots \circ P_{v_2}$.

Similarly, the restricted *Poincaré* map for the zero dynamics (as discussed in[43]) can be defined accordingly as $\rho_{v_i} : S^X_{e_{i-1}} \cap \mathbf{Z}_{v_{i-1}} \to S^X_{e_i} \cap \mathbf{Z}_{v_i}$ and more explicitly:

$$\rho_{v_i}(\xi_{v_{i-1}}) = \varphi_{\mathbf{Z}_{v_i}}(T_{\rho_{v_i}}(\Delta_{\mathbf{Z}_{e_{i-1}}}(\xi_{v_{i-1}}), \Delta_{\mathbf{Z}_{e_{i-1}}}(\xi_{v_{i-1}})), \quad (48)$$

where $\xi_{v_i} \in S^X_{e_i}|_{\mathbf{Z}_{v_i}}$; $\Delta_{\mathbf{Z}_{e_i}} = \Delta_{e_i}|_{\mathbf{Z}_{v_i}}$ is the restricted reset map for the zero dynamics and $T_{\rho_{v_i}}$ is the restricted time-to-impact function which is simply given by $T_{\rho_{v_i}}(\xi_0) = T_{I_{v_i}}(x_0|_{\mathbf{Z}})$. Particularly, the *Poincaré* return map for the multi-domain zero dynamics can be defined as:

$$\rho := \rho_{v_N} \circ \cdots \circ \rho_{v_1}, \quad (49)$$

and therefore ρ is also the *Poincaré* map for the hybrid zero dynamics system with a single-domain as defined in:[43]

$$\bar{\mathscr{H}}_{\mathbf{Z}} = (\bar{\mathbf{Z}}, \bar{S}_{\mathbf{Z}}, \bar{\Delta}_{\mathbf{Z}}, \bar{q}), \quad (50)$$

where $\bar{\mathbf{Z}} = \mathbf{Z}_{v_1}$, $\bar{S}_{\mathbf{Z}} = S^X_{e_1} \cap \mathbf{Z}_{v_1}$ and $\bar{\Delta}_{\mathbf{Z}} = \Delta_{\mathbf{Z}_{e_N}} \circ \rho_{v_N} \circ \cdots \circ \rho_{v_2}$, $\bar{q} = q_{v_1}$. Therefore, the invariance of the multi-domain hybrid zero dynamics which is guaranteed by the satisfaction the mutli-domain PHZD constraints as in (40) is equivalent to the invariance of the partial hybrid zero dynamics of single domain as in (50).

It is important to notice that this observation allows the results developed for single-domain models in[43] to be applied to models with multiple domains as in (2). With the assumption that the multi-domain hybrid system is C^1 in each domain and has a transversal periodic orbit $\mathscr{O}$,[34] we know that $\Delta = \Delta_{e_N} \circ P_{v_N} \circ \cdots P_{v_2}$ is continuous in a neighborhood of $x^* = \mathscr{O} \cap S^X$. Therefore, because of the results in Sect. 4.2.2 of[37] along with the assumption that the periodic orbit $\mathscr{O}$ is transversal, exponential stability of the multi-domain hybrid system can be checked by evaluating eigenvalues of the Jocobian of P at x^*. More importantly, due to the fact that a periodic orbit for the zero dynamics, $\mathscr{O}_{\mathbf{Z}}$, corresponds to a periodic orbit for the full-order dynamics, $\mathscr{O} = \iota_0(\mathscr{O}_{\mathbf{Z}})$, through the canonical embedding $\iota_0 : \mathbf{Z} \to D^X$ given by $\iota_0(\xi) = (\mathbf{0}, \xi)$, the exponential stability of the full order hybrid system can be guaranteed by the exponential stability of the reduced order hybrid system.

Therefore, the above framework of the reconstructed full- and reduced- order multi-domain hybrid system allow us to formally expand the results from[43] to the multi-domain situation by stating the following theorem:

Theorem 1. *Given the multi-domain hybrid system* (3)*, which can be reconstructed to a single-domain hybrid system as* (47)*, let $\mathscr{O}_Z$ be an exponentially stable transverse periodic orbit of the corresponding hybrid zero dynamics system* (50)*, then there exists $\varepsilon \in (0, 1)$ such that $\varepsilon = \min\{\varepsilon_1, \ldots, \varepsilon_N\}$ with each ε_i belonging to the set $(0, 1)$ for all the human-inspired controllers in each domain D_v as defined in* (32) *and* (34)*, $\mathscr{O} = \iota_0(\mathscr{O}_{\mathbf{Z}})$ is an exponentially stable periodic orbit for the full order dynamics of the multi-domain hybrid system* (2)*.*

Proof: The proof comes directly from the *Proposition 4* in[34] along with the proof in *Theorem 2* in[43] with the reconstructed single-domain hybrid zero dynamics system (50). From discussion in,[43] we know that the human-inspired controllers as defined in (32) and (34) are *Lipschitz continuous* and belong to the *rapidly exponential stable-control Lyapunov function* (RES-CLF) based control set K_ε as defined in,[43] which therefore illustrates the proof of this theorem. ∎

Application to AMBER2. Motivated by the fact that the multi-domain locomotion of AMBER2 consists one domain that is fully-actuated, we construct an equivalent single-domain hybrid system around this fully-actuated intermediate domain D_{R,v^i} as:

$$\mathscr{H}_R = (\bar{D}_R, \bar{S}_R, \bar{\Delta}_R, \bar{f}_R), \quad (51)$$

where $\bar{D}_R = D_{R,v^i}$, $\bar{f}_R = f^X_{R,v^i}$, $\bar{S}_R = S^X_{R,e^i_-}$ and $\bar{\Delta}_R = \Delta_{R,e^i_+} \circ P_{R,v^+} \circ P_{R,v^-}$. Combining the *Theorem 1* and the results from,[31] we propose the following corollary to show that satisfying the PHZD constraints yields formally provable stable gait for AMBER2.
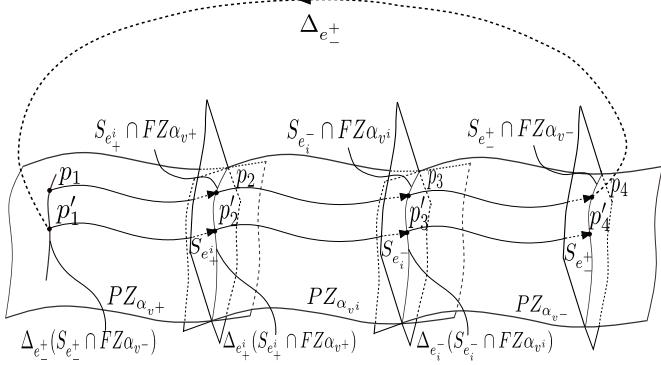
Fig. 9: Geometry of the closed-loop multi-domain system of AMBER2 evolving on the low dimensional PHZD surfaces with the human-inspired controllers discussed in this paper.

Corollary 1. *Given the hybrid system* (5) *which can be reconstructed to a single-domain hybrid system as* (51)*, let β^* be the parameters that satisfy the PHZD constraints as in* (40)*, then there exists $\varepsilon \in (0, 1)$ such that $\varepsilon = \min\{\varepsilon_1, \varepsilon_2, \varepsilon_3\}$ with each ε_i belonging to the set $(0, 1)$ for all the human-inspired controllers in each domain $D_{R,v}$ as defined in* (32) *and* (34)*, the multi-domain hybrid system has an exponential stable periodic orbit, $\mathscr{O}_\varepsilon$, which depends on ε.*

The detailed discussion along with the explicit construction of the PHZD constraints will be explained in the Appendix A. Note that, β is the expanded parameter set of α with two extra augment parameters which will not affect the PHZD constraints. The details will be illustrated in the Appendix A.

C. Multi-Domain Optimization

We now have necessary framework to present an optimization problem with the goal of finding the controller parameter set α, which delivers both human-like and stable multi-domain robotic walking. To achieve the goal of human-like locomotion, reference-data-based cost is adopted as the objective of the optimization problem. Specifically, the objective cost function is sum of the least squares fit errors between the robot outputs and the actual outputs of the reference walking behavior in each domain, which can be stated as follows:

$$\text{Cost}_{\text{REF}}(\alpha) = \sum_{i \in O_v} \sum_{k=1}^{K_i} \left(y_i^H[k] - y_i^d(t_i^H[k], \alpha_i) \right)^2, \quad (52)$$

where t_i^H and K_i are the discrete time and the number of discrete points for output $i \in O_v$, respectively. Note that for the purposes of this paper, we will continue to use data from two reference systems: human walking and SLIP locomotion.

The optimization problem is subject to two key types of constraints: PHZD constraints that ensure hybrid invariant of the partial zero dynamics through impacts, and physical constraints that guarantee the results are practical realizable. Given the cost function and the main constraints, the optimization

problem can be stated as the following:

$$\alpha^* = \text{argmin} \ \text{Cost}_{\text{REF}}(\alpha) \tag{HIO}$$
$$\text{s.t} \quad \Delta_e(S_e \cap \mathbf{PZ}_{\alpha_{sor(e)}}) \subset \mathbf{PZ}_{\alpha_{tar(e)}} \tag{PHZD}$$
$$\text{Physical Constraints} \tag{PHYC}$$

which we term the *human-inspired optimization* (HIO) problem due to the human-inspiration for generating the output functions that form the basis of the optimization. As discussed before, while this optimization problem is inspired by human locomotion (in the selection of outputs), it is not limited to human-locomotion data—nor even dependent on such data. Therefore, the end result of this generalized HIO problem is the control parameter set α that yields formal multi-domain bipedal locomotion while simultaneously guaranteeing that the obtained walking is as close to the reference system as possible. For example, the reference system can be the human locomotion system if the goal is to achieve human-like robotic multi-domain walking (AMBER2); and can also be a SLIP model if we want to achieve SLIP-like multi-domain locomotion (ATRIAS). Considering the space limits and structure simplicity, the explicit optimization constructions of both AMBER2 and ATRIAS are omitted here but can be found in Appendix A and B, respectively.

Example 13. With the HIO problem constructed as in Appendix A, the end result is that by utilizing the human locomotion data as a reference, a stable human-like multi-domain robotic walking gait is achieved for AMBER2. This gait was simulated using the human-inspired controllers as discussed in Sec. IV. The resulting phase portrait can be seen in Fig. 10, in which the period orbit corresponding to the walking gait is shown. The obtained robotic outputs are then compared with the human locomotion outputs in Fig. 11a and Fig. 11b, showing that the resulting robotic walking is remarkably human-like given the physical differences between the robot and human. To numerically validate the stability of the walking gait, the *Poincaré* return map[44] is utilized to prove the stability of this gait; in this case, the maximum eigenvalue is smaller than one ($0.3422e^{-8}$) indicating a stable walking gait is achieved.

Example 14. A walking gait for ATRIAS was generated through the SLIP-inspired optimization (63) discussed in Appendix B. The gait was then simulated using the human-inspired controllers introduced in Sec. IV. The resulting periodic orbits can be seen in Fig. 10. The robustness of the gait was also investigated; the system was simulated from a perturbed initial condition to show the output tracking convergence, as depicted in Fig. 11c. Finally, the stability of the gait was numerically verified. For $\varepsilon = 100$, the maximum magnitude of the *Poincaré* eigenvalues, 0.7135, is less than one, establishing the gait's stability.

Due to the SLIP-inspired nature of the optimization, the full-order model gait behavior was compared to the ideal SLIP model gait. Although they have different speeds and step lengths, simulation shows that the planar center of mass trajectory of the full-order gait exhibits patterns very similar to that of the SLIP gait, as illustrated in Fig. 11d. Note that the
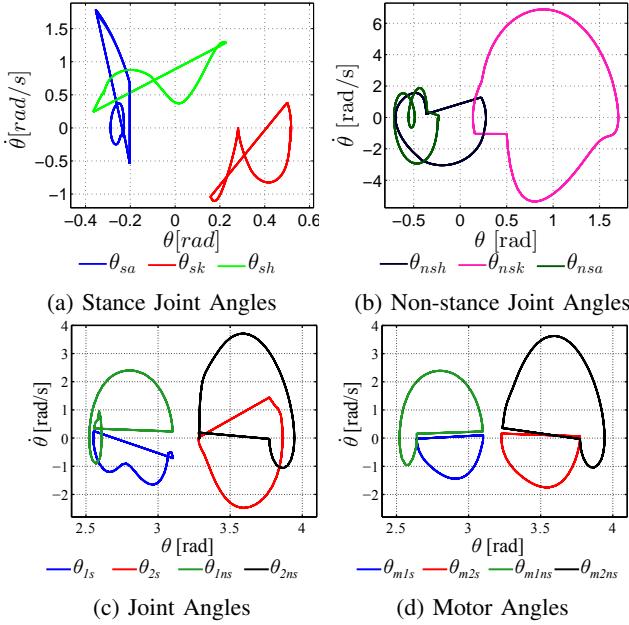
Fig. 10: Stable periodic orbits in the joint angles and motor angles for both AMBER2 (as shown in (a) and (b)) and ATRIAS (as shown in (c) and (d)). Note that the difference in shape between (c) and (d) demonstrate the compliance present in the robotic system being considered.
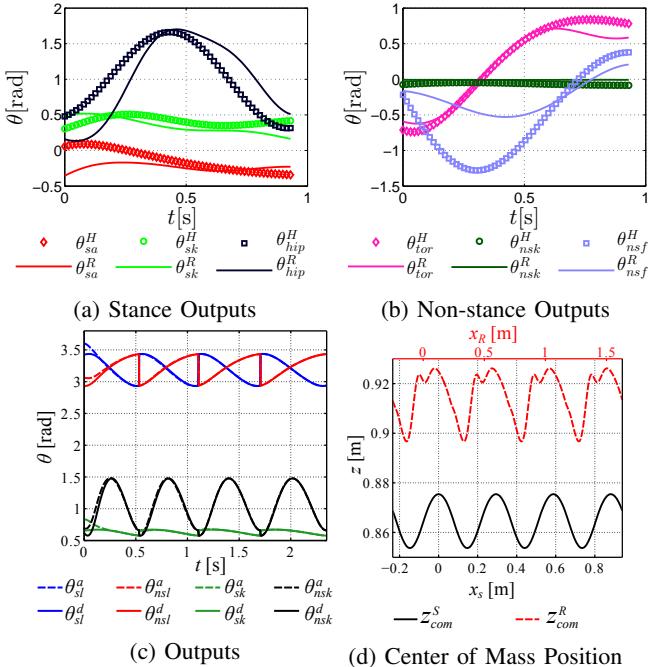

Fig. 11: Simulation results: (a) and (b) Comparisons between the human locomotion outputs and the robot outputs of AMBER2; (c) Desired versus actual outputs starting from a perturbed point of ATRIAS; (d) A comparison of the center of mass trajectory between the ideal SLIP gait and the full-order robotic model.

x positions of the two trajectories are on different scales. To show the similarities, the x-axis scaling was adjusted between

the two gaits so that they are in phase. This difference could be a result of the ideal SLIP model's massless leg assumption. In the SLIP model, the leg is assumed massless, enabling instantaneous changes in position during swing. Therefore, SLIP gaits with very short single support phases may not be physically possible with the full-order model. Moreover, to achieve sustainable walking on a real robot, a proper foot clearance constraint is needed with a maximum non-stance foot height. To satisfy this constraint, the optimization will tend to find gaits with a comparatively high center of mass position. Despite these differences, the full-order system's walking gait is remarkably SLIP-like.

VI. IMPLEMENTATION RESULTS

Having provided the formal methodology for generating multi-contact walking gaits, we now discuss the methodology for translating these results to physical robots. Through a procedure utilizing partial hybrid zero dynamics, we present a method for generating parameterized desired joint trajectories that allow for the experimental implementation on both AM-BER2 and ATRIAS with the end result being multi-contact locomotion.

A. Implementation on AMBER2

As the parameters α are designed for the outputs, it is necessary to use the PHZD reconstruction method discussed in Sec. V-A to resolve the desired joint trajectories $(\theta_d, \dot{\theta}_d)$ for practical realization. Tracking these joint trajectories would be equivalent to tracking the designed outputs. In order to obtain the PHZD reconstruction, both $\xi_{1,v}$ and $\xi_{2,v}$ can be computed based on the current state for each domain. However, as the hip velocity term $\xi_{2,v}$ is associated with multiple encoders, the actual value will accumulate the signal errors of all its contributing encoders. The end result will be inaccurate velocity data. To bypass this shortcoming, we exploit the advantages of the hybrid zero dynamics by solving the zero dynamics ODE shown in (42) explicitly as follows:

$$\xi_1(t) = \mathrm{v}_{hip}^* t + \frac{(1 - \exp(-\varepsilon t))}{\varepsilon}(v_{hip}^0 - \mathrm{v}_{hip}^*) + \delta p_{hip}^0,$$
$$\xi_2(t) = \mathrm{v}_{hip}^* + \exp(-\varepsilon t)(v_{hip}^0 - \mathrm{v}_{hip}^*),$$
$$\tag{53}$$

where δp_{hip}^0 and v_{hip}^0 are the initial hip position and hip velocity at the beginning of a step; v_{hip}^* is the desired hip velocity from optimization.

To establish state based tracking, the time t is replaced with the parametrized time $\tau(\theta)$, which is computed based on the current state that are read from the encoders. Note that, even though the output of hip velocity is not tracked during the under-actuated domain, it is still reasonable to achieve an approximation with this method considering the optimized trajectory. More detailed explanation can be found in.[21]

PD controllers are then used to track the joint angle and velocity profiles obtained from the PHZD reconstruction:

$$\tau_{PD} = -K_p(\theta^a - \theta^d) - K_d(\dot{\theta}^a - \dot{\theta}^d), \tag{54}$$

where K_p and K_d are proportional and derivative gain matrices, respectively. The proposed PD controller with the PHZD

(a) Human walking tiles for one step of high-stepping locomotion data.

(b) Simulated walking tiles for one step of AMBER2 with PD control.

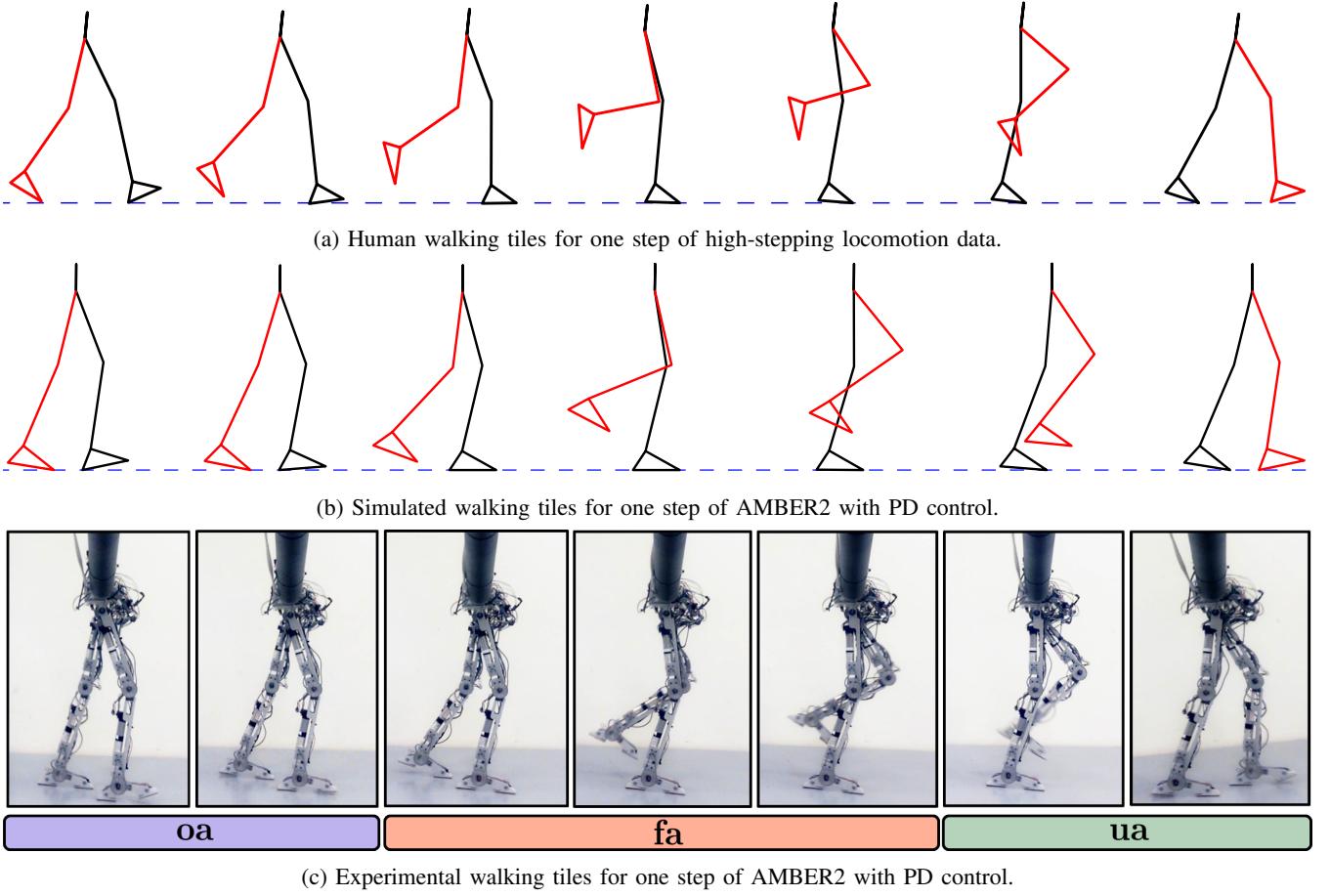(c) Experimental walking tiles for one step of AMBER2 with PD control.

Fig. 12: Comparison of walking tiles between the actual human walking, simulated walking and experimental walking.

reconstruction trajectories was verified in simulation before implementation on the physical robot. The simulation results generated using the human-inspired controller are presented in Fig. 13b. Comparing the human-inspired controller results as shown in Fig. 13a to the trajectories, we can observe that the PD controller with the reconstruction strategy has achieved similar results.

Experiment Setup. To realize real world walking on the physical robot AMBER2, LabVIEW 2011 is used for both the code development and robotic control. The controller for AMBER2 has two levels: a high level controller realized on a Real-Time (RT) module, and a low level controller implemented on a Field-Programmable Gate Array (FPGA), the details of which are explained in.[21]
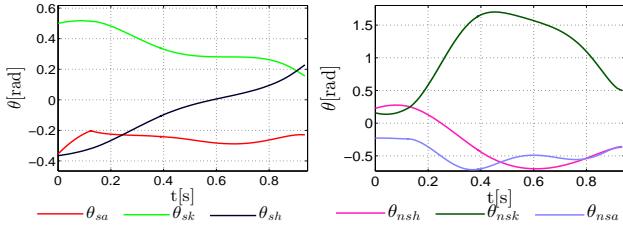
By applying a PD controller to track the reconstructed joint trajectories, AMBER2 has achieved sustainable human-like multi-domain walking. From the attached video as in,[21] the multi-domain walking of AMBER2 displays all the key features of human-like locomotion: toe strike, heel lift and heel strike. Particularly, AMBER2 has continuously walked for 45minutes with an approximated 1100m traveling distance. The test ended due to the mechanical failure of a driving chain. The commanded joint torques for each motor are shown in Fig. 14. The comparison between the experimental gait tiles and the simulated gait tiles is shown in Fig. 12. In particular, the actual reference high-stepping human locomotion data,

which we used to obtain the optimized trajectory, is also shown at the top of Fig. 12, revealing that the realized experimental walking is human-like. The actual joint angles obtained during an experiment are shown in Fig. 13c for comparison with the simulated results. These comparisons indicate that the robot replicates the formal result very well, i.e., there are good agreements between practice and theory. Robustness tests are performed to demonstrate that AMBER2 can sustain unintended pushes and overcome big obstacles.
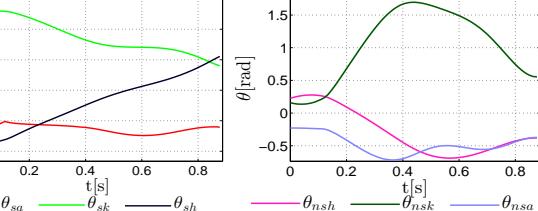
Also of note is that the system is developed with minimum sensing requirements by only using foot contact switches and incremental encoders. The inherent advantages imbibed in the ECWF—simpler form and better behavior outside of the nominal operation window, see[18] for more details—and the robot's design methodology facilitated the ease of applying such simple control laws to realize walking, which also resulted in low torque consumption throughout the step cycle. The actual joint angles of multiple steps along with the reconstructed desired joint trajectories are shown in Fig. 15.
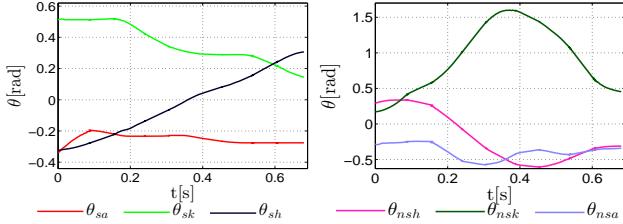
B. Implementation on ATRIAS

For practical realization, we want to find the desired robot motor angles and velocities at each iteration through inverse projection from the HZD surface. Recall that the outputs of the human-inspired controller are the linear mapping of the motor angles. Therefore, given the HZD surface determined

(a) Joint angles with IO control in simulation

(b) Joint angles with PD control in simulation

(c) Joint angles with PD control in experiment

Fig. 13: Comparison of actual joint angles between simulation and experimental results logged during AMBER2 walking.

by the parameter set α^* obtained from optimization, we can reconstruct the desired motor angles and velocities from the system outputs on the HZD surface in the same manner as discussed in (43). Because tracking the joint angles and velocities of the robot is equivalent to tracking the outputs, the restriction of the dynamics to the partial zero dynamics surface is maintained.

PD controllers are then used to track the desired motor angles and velocities obtained from the HZD reconstruction:

$$\tau_{PD} = -K_p(\theta_m^a - \theta_m^d) - K_d(\dot{\theta}_m^a - \dot{\theta}_m^d), \qquad (55)$$

where K_p and K_d are proportional and derivative constant matrices, respectively. Here, the elements of the K_p and K_d matrices depend on their corresponding motors.

Experiment Setup. ATRIAS is supported by a boom that constrains it to the sagittal plane so as to emulate a 2D planar robot. In addition, boom encoders at each degree of freedom provide feedback on the robot's torso position and rotation relative to the world frame. During experiments the boom also functions as a safety mechanism to catch the robot in the event of a fall; it does not provide any support in the sagittal plane at any other time.

Each experiment was conducted in a similar manner. The control system was initially enabled while ATRIAS was suspended in the air, allowing the software to drive the robot to an initial pose. ATRIAS was then lowered to the ground and manually given an initial impulse to initiate the walking motion. Fig. 16 and Fig. 17 show the tracking of the motor
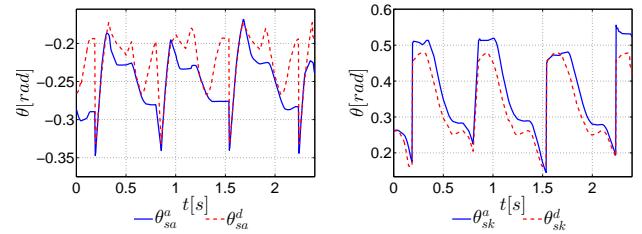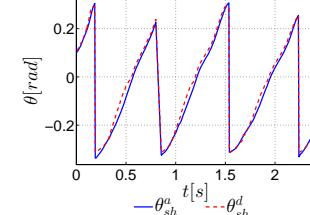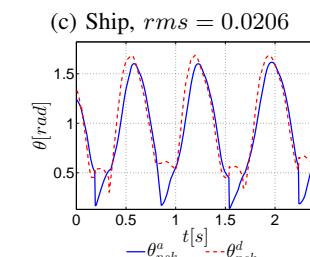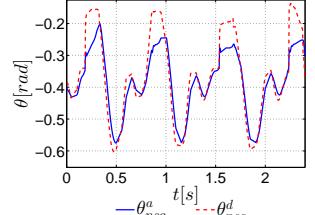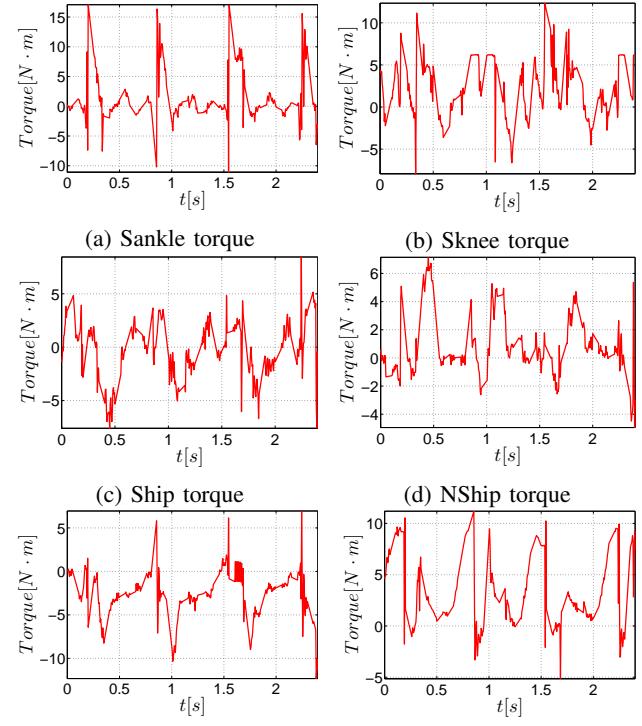

(a) Sankle, $rms = 0.0459$

(b) Sknee, $rms = 0.0457$

(c) Ship, $rms = 0.0206$

(d) NShip, $rms = 0.0435$

(e) NSknee, $rms = 0.2033$

(f) NSankle, $rms = 0.0567$

Fig. 14: Actual vs. desired joint angles logged during AM-BER2 walking with the unified control law, with rms the root mean square of tracking error.

(a) Sankle torque

(b) Sknee torque

(c) Ship torque

(d) NShip torque

(e) NSknee torque

(f) NSankle torque

Fig. 15: Torque inputs of each motor

(a) θ_{m1L}, $rms = 0.0169$

(b) θ_{m2L}, $rms = 0.0355$

(c) θ_{m1R}, $rms = 0.0162$

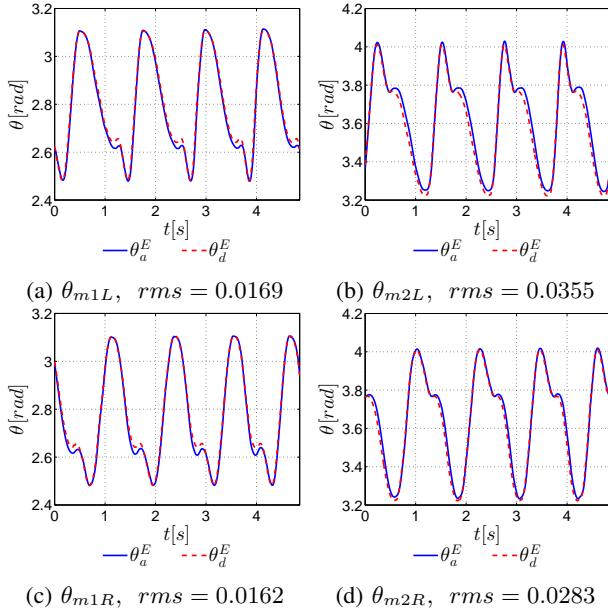(d) θ_{m2R}, $rms = 0.0283$

Fig. 16: Comparison of the actual θ_a^E versus desired θ_d^E motor angle trajectories of left leg $(\theta_{m1L}, \theta_{m2L})$ and right leg $(\theta_{m1R}, \theta_{m2R})$ from experiment.

(a) $\dot{\theta}_{m1L}$, $rms = 0.2664$

(b) $\dot{\theta}_{m2L}$, $rms = 0.2855$

(c) $\dot{\theta}_{m1R}$, $rms = 0.1660$
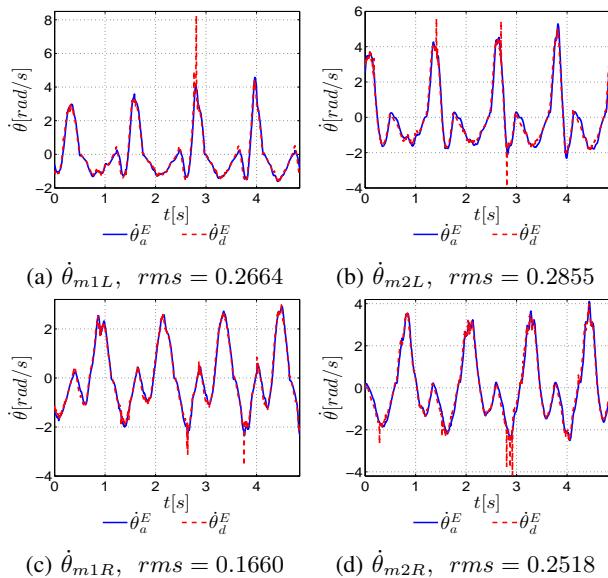
(d) $\dot{\theta}_{m2R}$, $rms = 0.2518$

Fig. 17: Comparison of actual $\dot{\theta}_a^E$ vs. desired $\dot{\theta}_d^E$ motor velocities trajectories of left leg $(\dot{\theta}_{m1L}, \dot{\theta}_{m2L})$ and right leg $(\dot{\theta}_{m1R}, \dot{\theta}_{m2R})$ from experiment.

angles and velocities of the left and right legs during four walking steps with the left leg as the stance leg for the first step. The corresponding input torques for each motor are shown in Fig. 18. Note that the subscripts 'L' and 'R' in the subtitles represent the left and right leg, respectively. The tracking errors are exceptionally small with motor torque inputs remaining within the robot's capabilities. The end result is a dynamically stable walking gait that visually appears "SLIP-like". The snapshots in Fig. 19 illustrate the extraordinary similarities between the simulated and experimental gaits. The video of the experiment shows sustainable walking with
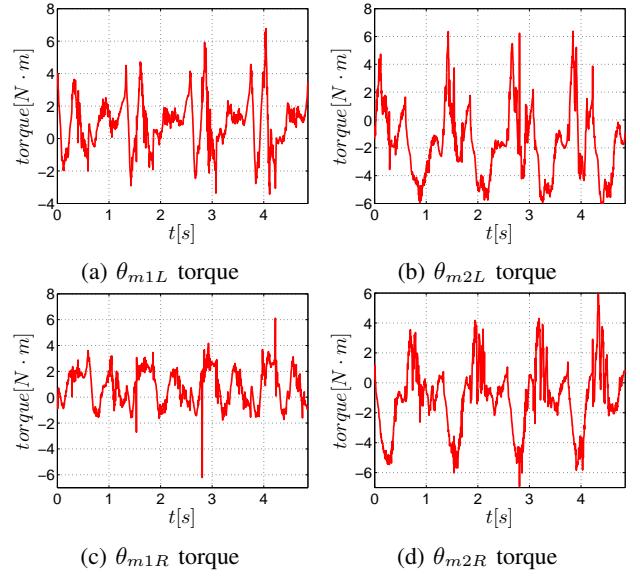

(a) θ_{m1L} torque

(b) θ_{m2L} torque

(c) θ_{m1R} torque

(d) θ_{m2R} torque

Fig. 18: Torque inputs of each motor.

ATRIAS and is available in.[26]

VII. CONCLUSIONS

The main contribution of this paper is to present a general formal means by which multi-domain bipedal robotic locomotion was achieved first in simulation and finally on two physical robots, AMBER2 and ATRIAS. With the goal of formally establishing stable bipedal robotic walking, a theorem utilizing the framework of hybrid zero dynamics and *Poincaré* return map techniques is proposed for the first time, according to which the exponential stability of the full order hybrid system can be guaranteed by the exponential stability of the reduced order hybrid system. This theorem is then extended to the case of AMBER2 showing that the exponential stability of the reduced order hybrid system can be achieved within the framework of the multi-domain hybrid system of AMBER2. The end result of this framework implementation is the formally stable multi-contact walking.

To verify the theorem analysis onto the physical robot platforms, the main goals of this work are achieved with the following steps. With the human locomotion as the reference, a novel multi-domain optimization was developed first to generate control parameters that yield stable and human-like multi-domain locomotion. In order to realize this result on a physical robot, the PHZD trajectory reconstruction methodology was then utilized to generate joint trajectories for robust tracking while at the same time restricting the dynamics to the invariant hybrid zero dynamic surface. With the experimental implementation inheriting the essential formal elements of the controllers and optimization, which are utilized to generate these gaits, stable robotic walking that displays qualitatively human-like walking with distinct multi-contact behaviors in a dynamic fashion is realized. Robustness tests showed that the walking was robust to various disturbances and can walk over obstacles for a wide range of heights.

While this complete methodology was inspired from human locomotion, it was not limited to human-locomotion data—nor

even depend on human data. With the SLIP model as the reference, this methodology was successfully utilized to generate a multi-domain SLIP-like walking gait and implemented on the robot ATRIAS with the results of achieving stable multi-domain SLIP-like locomotion.

Note that it is the PHZD based optimization problem and trajectory reconstruction that bridges the gap between the theory and experimentation. The work in this paper is only focused on planar multi-domain locomotion with less than four domains. However, it is also applicable to add more domains or expand to $3D$ locomotion (more sets of parameters will be required) with the PHZD surfaces being properly constructed. PHZD $3D$ multi-domain locomotion will be the focus of future work on this topic.

APPENDIX A:
OPTIMIZATION CONSTRUCTION OF AMBER2

This section will discuss the detailed construction of the multi-domain optimization for AMBER2 by considering the PHZD constraints for each transition.

Intermediate to Pre-Impact Constraints. In order to reframe the PHZD constraints in a way such that the optimization problem can be numerically approached, we use the PHZD reconstruction strategy to construct a point $(\upsilon, \dot{\upsilon}) \in \mathbf{PZ}_{v^i} \cap S^X_{e^i_-}$, and due to the full control authority, we know that $\xi_{2,v^i} = v_{hip}$. Next, we add an additional parameter by defining $\xi_{1,v^i} = \alpha^{v^i}_{p_{hip}}$ to obtain the hip position ξ_{1,v^i}. Therefore, we expand our set of parameters by defining: $\beta_{v^i} = \{\alpha^{v^i}_{p_{hip}}, \alpha_{v^i}\}$. By doing so, we can explicitly solve the point $(\upsilon(\beta_{v^i}), \dot{\upsilon}(\beta_{v^i}))$ as $\upsilon(\beta_{v^i}) = \Psi(\alpha^{v^i}_{p_{hip}}, \alpha_{v^i})$ and $\dot{\upsilon}(\beta_{v^i}) = \Phi(\alpha^{v^i}_{p_{hip}}, v_{hip}, \alpha_{v^i}))$.

With this construction, we can specifically impose the constraint of domain v^i, which indicates that the reaction force on the heel has to cross zero,

$$h_{v^i}(\upsilon(\beta_{v^i}), \dot{\upsilon}(\beta_{v^i})) = 0. \qquad \text{(RC1)}$$

Note that, the intermediate domain v^i will switch to the pre-impact domain v^- smoothly without requiring any further constraints except the guard condition. This is the benefit of using only one ECWF through all three domains. Particularly, with the addition parameter $\alpha^{v^i}_{p_{hip}}$, the time of the switch moment $S^X_{e^i_-}$ can also be optimized.

Pre-Impact to Post-Impact Constraints. The constructed point $(\upsilon(\beta_{v^i}), \dot{\upsilon}(\beta_{v^i})) \in \mathbf{PZ}_{v^i} \cap S^X_{e^i_-}$ above is also the initial point of domain v^- due to the fact $\Delta_{e^i_-} = I$, i.e., the reset map of this transition is identity. With φ^{v^-} denoting the solution of the vector (f_{v^-}, g_{v^-}), we can define the following point:

$$(\varphi(\beta_{v^i}), \dot{\varphi}(\beta_{v^i})) = \varphi^{v^-}_{T_{v^-}(\upsilon(\beta_{v^i}), \dot{\upsilon}(\beta_{v^i}))}(\upsilon(\beta_{v^i}), \dot{\upsilon}(\beta_{v^i})). \quad \text{(56)}$$

Clearly, $(\varphi(\beta_{v^i}), \dot{\varphi}(\beta_{v^i})) \in S^X_{e^-_+}$. In order to satisfy the PHZD constraints, the post impact state of $(\varphi(\beta_{v^i}), \dot{\varphi}(\beta_{v^i}))$ has to be on the surface of $\mathbf{PZ}_{v^+}$, which implies the following constraints:

$$y_{2,v^+}(\Delta_{\theta,e^-_+} \varphi(\beta_{v^i})) = 0, \qquad \text{(RC2)}$$

$$dy_{2,v^+}(\Delta_{\theta,e^-_+} \varphi(\beta_{v^i}))\Delta_{\dot{\theta},e^-_+} \dot{\varphi}(\beta_{v^i}) = 0, \qquad \text{(RC3)}$$

$$\frac{\partial h_{v^-}(\varphi(\beta_{v^i}))}{\partial \varphi(\beta_{v^i})} \dot{\varphi}(\beta_{v^i}) < 0, \qquad \text{(RC4)}$$

where constraint (RC4) implies that the impact is transverse to the guard. [35]

Post-impact to Intermediate Constraints. Analogous to the PHZD reconstruction at the end of domain v^i, we seek to construct a point $(\upsilon, \dot{\upsilon}) \in \mathbf{PZ}_{v^+} \cap S^X_{e^i_+}$ with an additional parameter $\alpha^{v^+}_{p_{hip}}$ denoting the hip position at the end of domain v^+. Note that, with the assumption that the controller gain ε is large enough to drive the actual hip velocity to the desired value with sufficient speed (before the end of domain v^+), we have $\xi_{2,v^+} = v_{hip}$. Therefore, by defining the extended parameter set to be $\beta_{v^+} = \{\alpha^{v^+}_{p_{hip}}, \alpha_{v^+}\}$, we can solve for this point as $\upsilon(\beta_{v^+}) = \Psi(\alpha^{v^+}_{p_{hip}}, \alpha_{v^+})$ and $\dot{\upsilon}(\beta_{v^+}) = \Phi(\alpha^{v^+}_{p_{hip}}, v_{hip}, \alpha_{v^+})$.

Finally, we can explicitly compute the point at the beginning of the domain v^i using the reset map $\Delta_{e^i_+}$ with $\Delta_{\theta,e^i_+} = I$ and $\Delta_{\dot{\theta},e^i_+}$ as discussed in (18). Thence, the specific constraints for the minor impact transition can be stated as follows:

$$y_{\{hip,tor\},v^i}(\upsilon(\beta_{v^i})) = 0, \qquad \text{(RC5)}$$

$$|dy_{2,v^i}(\upsilon(\beta_{v^+}))\Delta_{\dot{\theta},e^i_+} \dot{\upsilon}(\beta_{v^+})| < \sigma, \qquad \text{(RC6)}$$

$$\frac{\partial h_{v^+}(\upsilon(\beta_{v^+}))}{\partial \upsilon(\beta_{v^+})} \dot{\upsilon}(\beta_{v^+}) < 0, \qquad \text{(RC7)}$$

where (RC7) implies that the impact is transverse to the guard. The constant σ is a small positive user-defined value, which is chosen to be 0.1 in our application. Note that, since only one ECWF has been utilized to characterize the outputs of a whole gait cycle, the PHZD surface can not be fully guaranteed throughout the whole step, which contains three domains and two impacts. Therefore, the PHZD constraints for the switch between the post-impact domain v^+ and the intermediate domain v^i have to be relaxed by only constraining the positions of the outputs, i.e., the states are allowed to be off the PHZD surface for a small moment right after the minor impact. Therefore, the constraints (RC6) make sure that the velocity changes due to the minor impact of the toe strike are smaller than a specific value. As a result, the system will not be thrown off the PHZD surface too much and will converge back to the surface sufficiently quick. In particular, since the shared position modulating outputs between domain v^+ and v^i will be continuous by construction due to the identity position reset map, constraints (RC5) enforce that the outputs y_{hip,v^+} and y_{tor,v^+} which are not tracked during the domain v^+ should be on the surface of $\mathbf{PZ}_{v^i}$.

Physical Constraints. Despite the PHZD constraints which insure a stable periodic orbit for the considered hybrid system, [35] we also consider several physical constraints such that the results of the optimization are in a form that can be implemented on the physical robots directly. In particular, the
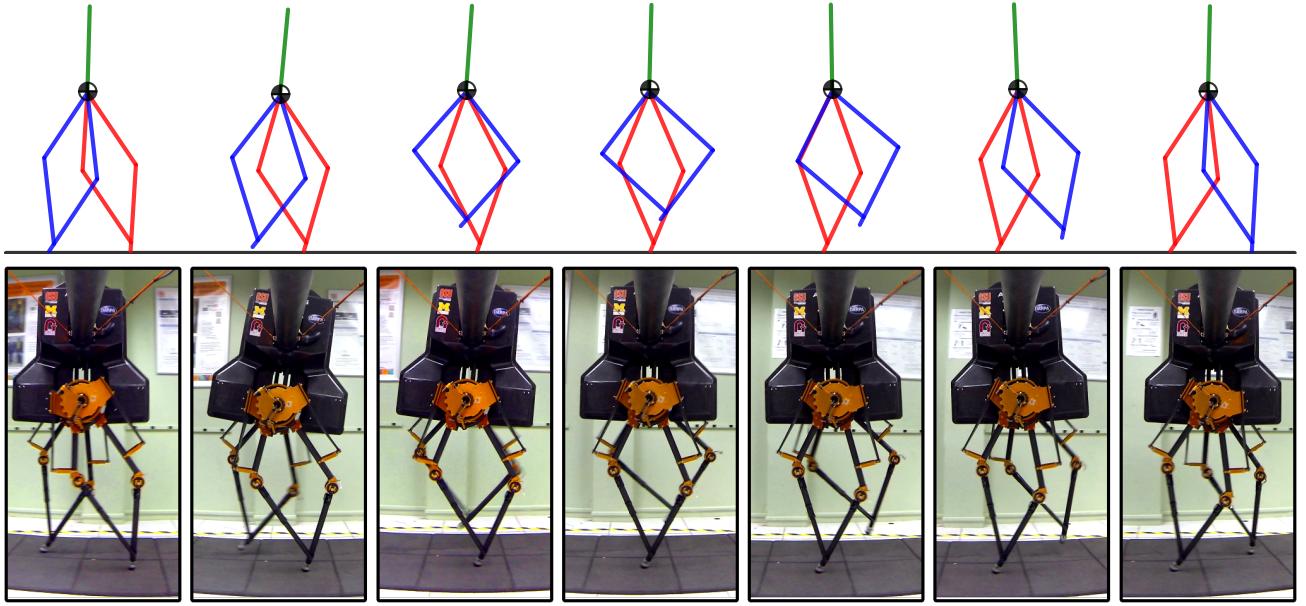
Fig. 19: Walking gait snapshot comparison of the simulation and experimental results with ATRIAS over one step.

following two types of physical constraint are considered:

Torque Constraints. Torques acting on the joints are limited by the capacity of the motors and the motion control modules. Therefore, the optimized gait has to respect the hardware torque bounds, which is stated as:

$$\max_{0 \leq \tau(\theta(\beta))} ||u(\theta(\beta), \dot{\theta}(\beta), \varepsilon)|| \leq MAX_{torque}, \qquad \text{(RC8)}$$

where $\beta = \{\alpha_{p_{hip}}^{v^+}, \alpha_{p_{hip}}^{v^i}, \alpha\}$ is the final expanded parameter set.

Foot Scuffing Conditions. The swing height clearance of toe and heel, and stride length during the swing phase must be sufficient to avoid scuffing amidst sensor noise, tracking error, uneven ground and even imperfections in the mechanical design. Therefore, foot scuffing conditions must be imposed to insure sustainable walking. Explicitly, we define:

$$\max_{0 \leq \tau(\theta(\beta))} (h_{nst}(\theta(\beta)) - h_{quad}(\theta(\beta), hmax)) > 0,$$
$$\max_{0 \leq \tau(\theta(\beta))} (h_{nsh}(\theta(\beta)) - h_{quad}(\theta(\beta), hmax)) > 0,$$
$$\max_{0 \leq \tau(\theta(\beta))} l_{nsf}(\theta(\beta)) - MIN_{steplength} > 0, \qquad \text{(RC9-11)}$$

where h_{quad} is a quadratic polynomial above which the height of non-stance toe (h_{nst}) and heel (h_{nsh}) must remain during the course of a step. The stride length l_{nsf} is constrained to be greater than a minimum specified stride length, $MIN_{steplength}$.

Main Results. Utilizing all of the formal constructions above, together with the constraints needed for practical implementation, the final multi-domain optimization problem for AM-

BER2 can be stated as:

$$\beta^* = \operatorname*{argmin}_{\beta \in \mathbb{R}^{45}} \text{Cost}_{\text{HD}}(\beta) \qquad \text{(HIO)}$$
$$\text{s.t} \quad \text{PHZD} \quad \text{Constraints} \qquad \text{(RC1-7)}$$
$$\text{Physical} \quad \text{Constraints} \qquad \text{(RC8-11)}$$

where the human-data-based cost is defined as:

$$\text{Cost}_{\text{HD}}(\beta) = \sum_{i \in O_v} \sum_{k=1}^{K_i} \left(y_i^H[k] - y_i^d(t_i^H[k], \beta_i) \right)^2, \qquad \text{(57)}$$

with t_i^H and K_i being the discrete time and the number of discrete points for output $i \in O_v$, respectively. By solving this optimization problem , we can obtain the optimized β^* parameters that best fit human-walking data while enforcing the desired constraints to achieve stable multi-domain robotic walking as stated in *Corollary 1*. Note that, *Corollary 1* follows from the following observations coupled with the PHZD constructions in this section.

According to the *Theorem 1* in,[31] constraints RC2-4 guarantee that the system is invariant in the partial hybrid zero dynamics through the major impact, i.e., the heel strike. Another important fact of satisfying constraints RC2-4 is that we are able to make sure that under-actuated domain can complete one step by using the numerical integration through the course of under-actuated domain. More importantly, benefited from the fact that only one CWF is used for the whole step cycle, the system is thus invariant through the rest domain transitions. In particular, for AMBER2 walking with an extra small toe impact, constraints RC5-7 indicate that this impact is minor and transversal, insuring the system converges back to the partial hybrid system sufficiently quick. Therefore, with the folded one domain construction of AMBER2, we have $\Delta(S^X \cap \mathbf{PZ}_\beta) \subset \mathbf{PZ}_\beta$ with $\mathbf{PZ}_\beta$ being the partial hybrid zero dynamics of domain $D_{v^i}^X$. According to the *Theorem 2* in,[31]

the hybrid system (5) has an exponentially stable periodic.

APPENDIX B:
OPTIMIZATION CONSTRUCTION OF ATRIAS

SLIP Inspired Optimization. This section utilizes the fact that the *zero dynamic surfaces* in (35) are invariant under the flow of closed-loop continuous dynamics while not necessarily invariant for the discrete dynamics. In particular, the invariance of the zero dynamics will be disturbed at the discrete impacts that occur as a result of contact points changing. For the hybrid system of ATRIAS, the only impact occurs when the robot transitions from the *single support* domain into the *double support* domain. The goal of this section is to find a parameter set α^*, which guarantees hybrid invariance of the hybrid system of ATRIAS while tracking the center of mass (CoM) trajectory of SLIP model as close as possible. In particular, we construct the following constrained optimization problem, called *SLIP Inspired Optimization*:

$$\alpha^* = \underset{\alpha \in \mathbb{R}^{4 \times 5}}{\operatorname{argmin}} \ \text{Cost}_{\text{SLIP}}(\alpha), \tag{58}$$

$$\text{s.t} \quad \Delta_{e_-^+}(S_{e_-^+}^X \cap \mathbf{PZ}_{\alpha_{v-}}) \subset \mathbf{PZ}_{\alpha_{v+}} \tag{HZD}$$

with the SLIP-model-based cost function defined as:

$$\text{Cost}_{\text{SLIP}}(\alpha) = \tag{59}$$
$$\sum_{k=1}^{K} \sum_{i \in \{x,z\}} \left(p_{com,i}^{S}[k] - p_{com,i} \left(y_{ecwf}(t^S[k], \alpha) \right) \right)^2,$$

where discrete times, $t^S[k]$, and discrete values of the CoM position for the SLIP gait, $p_{com,i}^S[k]$, for $i \in \{x, z\}$, and $p_{com}\left(y^H(t^S[k], \alpha) \right)$ is the approximate CoM position of the robot computed from the outputs characterized by the ECWF. The end result is the least square fit of the CoM trajectory of the robot to that of SLIP model. In other words, we seek to "shape" the dynamics of the robot as close to the SLIP model dynamics as possible. Importantly, as illustrated before, because of ATRAIS is under-actuated through all domains, the partial zero dynamics $\mathbf{PZ}_{\alpha_v}$ is actually the full zero dynamics $\mathbf{Z}_{\alpha_v}$ for ATRIAS by definition. Therefore, we will use $\mathbf{PZ}_{\alpha_v}$ for this case to keep notation simple and consistent.

Hybrid Zero Dynamics. As discussed in previous section, a hybrid system has *hybrid zero dynamics* (HZD) if the zero dynamics are invariant through the impact. For a fully-actuated or over-actuated system, the pre-impact states can be explicitly solved for in terms of the parameter α using the inverse kinematics strategy directly.[35] However, because the system being considered has series elastic actuators, it is unable to be solved explicitly due to the high dimensions of the zero dynamics surface of the system. This difficulty stems from the fact that the pre-impact states of the zero dynamics coordinates need to be solved by integrating the dynamics defined in (38).

We assume that a set of points $(\theta_z^-, \dot{\theta}_z^-)$ are the local coordinates of the zero dynamics on the guard. Due to the fact that the guard function $h_{v^-}(\theta)$ only depends on the rigid body configurations, which is the same as (θ_z) in this case,

the following constraints need to be satisfied:

$$h_{v^-}(\theta_z^-) = 0, \tag{SC1}$$

$$dh_{v^-}(\theta_z^-)\dot{\theta}_z^- < 0, \tag{SC2}$$

where (SC2) guarantees that the guard is transversal. Note that, because of the special case of ATRIAS, the normal form of zero dynamics is exactly the equations of motion defined with the original state space. Therefore, we could choose the uncontrolled zero coordinates as $\eta = \theta_z \in \mathbf{Z}$ explicitly.

Now we expand our parameter set by defining, $\beta := \{\alpha, \theta_z^-, \dot{\theta}_z^-\}$. The advantage of this definition is that we can solve the pre-impact states explicitly in the terms of β, and simplify the constraints to the same form as in.[35] A point $(\vartheta(\beta), \dot{\vartheta}(\beta)) \in S_{e_+^-}^X \cap \mathbf{PZ}_{\alpha_{v-}}$ depending on these parameters can be obtained by solving the equations:

$$\vartheta(\beta) := \theta \quad \text{s.t.} \quad y(\Delta_{\theta, e_+^+}\theta) = \mathbf{0}_4, \tag{60}$$

$$\dot{\vartheta}(\beta) = Y^{-1}(\vartheta(\beta)) \begin{bmatrix} \dot{\theta}_z^- \\ \mathbf{0}_4 \end{bmatrix}, \tag{61}$$

where,

$$Y(\vartheta(\beta)) = \begin{bmatrix} H_z \\ dy(\vartheta(\beta)) \end{bmatrix},$$

with H_z being defined as

$$\theta_z = [\mathbf{I}_{7 \times 7} \quad \mathbf{0}_{7 \times 4}]\theta := H_z \theta. \tag{62}$$

The equation (60) is easy to solve using the fact that $\theta^+ = \mathcal{R}\Delta_{\theta, e_+^+}\theta$ and $\tau(\mathcal{R}\Delta_{\theta, e_+^+}\theta) = 0$ which imply: $y(\theta^+) = y^a(\theta^+) - y^d(0)$. With the proper choice of the outputs, the matrix $Y(\vartheta(\beta))$ is invertible. Thus the (HZD) of the system can be stated as,

$$y(\vartheta(\beta)) = \mathbf{0}, \tag{SC3}$$

$$dy\left(\mathcal{R}\Delta_{\theta, e_-^+}\vartheta(\beta) \right) \mathcal{R}\Delta_{\dot{\theta}, e_-^+}(\vartheta(\beta))\dot{\vartheta}(\beta) = \mathbf{0}, \tag{SC4}$$

which guarantees the hybrid invariance of the system through the impact.[35]

Physical Constraints. To achieve a physically permissible bipedal walking gait, several physical constraints are imposed on the optimization. The computations of the physical constraints are performed by integrating the zero dynamics of (38) over both *double support* and *single support* domains with the initial condition $\Delta_{e_-^+}(\vartheta(\beta), \dot{\vartheta}(\beta))$. Those constraints are addressed explicitly as follows:

Ground Reaction Forces: For the *double support* domain, the normal ground reaction forces on non-stance foot should be positive to prevent the reaction force actually "pulling" the robot against the ground, i.e.,

$$F_{ns}^z(\theta_z, \dot{\theta}_z, \alpha) > 0, \quad (\theta_z, \dot{\theta}_z) \in \mathbf{PZ}_{\alpha_{v+}}|\mathbf{z}. \tag{SC5}$$

For the *single support* domain, the normal ground reaction forces on stance foot should be positive, i.e., the stance foot should be in contact with the ground. Therefore, we require:

$$F_s^z(\theta_z, \dot{\theta}_z, \alpha) > 0, \quad (\theta_z, \dot{\theta}_z) \in \mathbf{PZ}_{\alpha_{v-}}|\mathbf{z}. \tag{SC6}$$

Friction: To prevent the stance foot from sliding, the following constraint is imposed:

$$F_s^x(\theta_z, \dot{\theta}_z, \alpha) < \mu F_s^z(\theta_z, \dot{\theta}_z, \alpha), \qquad \text{(SC7)}$$

where μ is the coefficient of static friction for the contact between stance foot and the ground.

Foot Clearance: From the definition of the D_{v^-}, the height of the non-stance foot needs to be above the ground during the *single support* domain. Using the fact that the height of the non-stance foot is the function of joint angles, we obtain:

$$h_{ns}(\theta_z) > 0, \quad (\theta_z, \dot{\theta}_z) \in \mathbf{PZ}_{\alpha_{v^-}}|\mathbf{z}. \qquad \text{(SC8)}$$

Touch Down Angle: To achieve stable walking with the ideal SLIP model, the touch down angle $\varphi_{\text{TD}}(\vartheta(\beta))$ (the angle of attack) needs to be a certain value. Therefore, to match the SLIP model dynamics as closely as possible, we impose a constraint on the touch down angle φ_{TD} such that it is equal to the desired value of the stable SLIP walking gait:

$$\varphi_{\text{TD}}(\vartheta(\beta)) = \alpha_{\text{TD}}. \qquad \text{(SC9)}$$

We now have the necessary framework in which to restate the multi-domain *SLIP Inspired Optimization* problem:

$$\beta^* = \underset{\beta \in \mathbb{R}^{36}}{\text{argmin}} \ \text{Cost}_{\text{SLIP}}(\beta) \qquad \text{(63)}$$

$$\text{s.t} \quad \text{PHZD} \quad \text{Constraints} \qquad \text{(SC1-4)}$$

$$\text{Physical} \quad \text{Constraints} \qquad \text{(SC5-9)}$$

The end result is a stable multi-domain walking gait with $\beta = (\alpha, \theta_z^-, \dot{\theta}_z^-)$ consisting of the parameters of the human walking function α, and the pre-impact state $(\theta_z^-, \dot{\theta}_z^-)$ of the zero dynamics. The stability of the gait is validated numerically through the use of the *Poincaré* map for the zero dynamics after the optimization which can be referred to.[26]

References

1. D. H. Sutherland, K. R. Kaufman, and J. R. Moitoza. "Human Walking". Williams & Wilkins Baltimore (1994).
2. M. Ackermann. "Dynamics and Energetics of Walking with Prostheses". PhD thesis University of Stuttgart Stuttgart (2007).
3. V. T. Inman and J. Hanson. "Human Locomotion". J. Rose and J. G. Gamble, editors, *Human Walking*. Williams & Wilkins Baltimore (1994).
4. A. D. Kuo. "Energetics of Actively Powered Locomotion Using the Simplest Walking Model". *Journal of Biomechanical Engineering* **124**(1), 113–120 (2001).
5. R. Sellaouti, O. Stasse, S. Kajita, K. Yokoi, and A. Kheddar. "Faster and Smoother Walking of Humanoid HRP-2 with Passive Toe Joints". *Intelligent Robots and Systems, 2006 IEEE/RSJ International Conference on* 4909–4914 (2006).
6. D. Tlalolini, C. Chevallereau, and Y. Aoustin. "Comparison of different gaits with rotation of the feet for a planar biped". *Robotics and Autonomous Systems* **57**(4), 371 – 383 (2009).
7. C. Chevallereau, D. Djoudi, and J. W. Grizzle. "Stable bipedal walking with foot rotation through direct regulation of the zero moment point". *Robotics, IEEE Transactions on* **24**(2), 390–401 (2008).
8. J. Lack, M. J. Powell, and A. Ames. "Planar Multi-Contact Bipedal Walking Using Hybrid Zero Dynamics". *Proceedings of IEEE International Conference on Robotics and Automation* 2582 – 2588 (2014).
9. N. Handharu, J. Yoon, and G. Kim. "Gait pattern generation with knee stretch motion for biped robot using toe and heel joints". *Humanoid Robots 8th IEEE-RAS International Conference on* 265–270 (2008).
10. Q. Huang, K. Yokoi, S. Kajita, K. Kaneko, H. Arai, N. Koyachi, and K. Tanie. "Planning Walking Patterns for a Biped Robot". *IEEE Transactions on Robotics and Automation* **17**, 280–289 (2001).
11. G. Bessonnet, P. Seguin, and P. Sardain. "A parametric optimization approach to walking pattern synthesis". *The International Journal of Robotics Research* **24**(7), 523–536 (2005).
12. K. Nishiwaki, S. Kagami, Y. Kuniyoshi, M. Inaba, and H. Inoue. "Toe joints that enhance bipedal and fullbody motion of humanoid robots". *Robotics and Automation, 2002. Proceedings. ICRA '02. IEEE International Conference on*, **3** 3105–3110 (2002).
13. Z. Li, B. Vanderborght, N. Tsagarakis, and D. Caldwell. "Human-like walking with straightened knees, toe-off and heel-strike for the humanoid robot iCub". *Control 2010, UKACC International Conference on* 1–6 (2010). doi: 10.1049/ic.2010.0356.
14. J. J. Alcaraz-Jiménez, D. Herrero-Pérez, and H. Martínez-Barberá. "Robust feedback control of ZMP-based gait for the humanoid robot Nao". *The International Journal of Robotics Research* **32**(9-10), 1074–1088 (2013).
15. K. Mitobe, G. Capi, and Y. Nasu. "Control of walking robots based on manipulation of the zero moment point". *Robotica* **18**(6), 651–657 (2000).
16. D. Tlalolini, C. Chevallereau, and Y. Aoustin. "Human-Like Walking: Optimal Motion of a Bipedal Robot With Toe-Rotation Motion". *Mechatronics, IEEE/ASME Transactions on* **16**(2), 310–320 (2011). ISSN 1083-4435. doi: 10.1109/TMECH.2010.2042458.
17. S. N. Yadukumar, M. Pasupuleti, and A. Ames. "From Formal Methods to Algorithmic Implementation of Human Inspired Control on Bipedal Robots". *10th International Workshop on the Algorithmic Foundations of Robotics*, **86** 511–526 (2012).
18. H. Zhao, M. Powell, and A. Ames. "Human-Inspired Motion Primitives and Transitions for Bipedal Robotic Locomotion in Diverse Terrain". *Optimal Control Applications and Methods* **35**(6), 730–755 (2013).
19. W. Ma, H. Zhao, S. Kolathaya, and A. Ames. "Human-

Inspired Walking via Unified PD and Impedance Control". *Proceedings of International Conference on Robotic and Automation* 5088 – 5094 (2014).

20. A. Ames, E. Cousineau, and M. Powell. "Dynamically Stable Robotic Walking with NAO via Human-Inspired Hybrid Zero Dynamics". *Proceedings of 15th ACM International Conference on Hybrid Systems: Computation and Control* 135–44 (2012).

21. H. Zhao, W.-L. Ma, M. B. Zeagler, and A. Ames. "Human-Inspired Multi-Contact Locomotion with AMBER2". *Proceedings of ACM/IEEE, International Conference on Cyber Physics System* 199–210 (2014).

22. J. A. Grimes and J. W. Hurst. "The design of ATRIAS 1.0 a unique monoped, hopping robot". *Proceedings of the 2012 International Conference on Climbing and Walking Robots and the Support Technologies for Mobile Machines* 548–554 (2012).

23. J. Hurst, J. Chestnutt, and A. Rizzi. "The Actuator With Mechanically Adjustable Series Compliance". *Robotics, IEEE Transactions on* **26**(4), 597–606 (2010).

24. A. Ames, R. Vasudevan, and R. Bajcsy. "Human-Data Based Cost of Bipedal Robotic Walking". *Proceedings of the 14th international conference on Hybrid systems: computation and control* 153–162 (2011).

25. J. A. Blaya and H. Herr. "Adaptive control of a variable-impedance ankle-foot orthosis to assist drop-foot gait". *Neural Systems and Rehabilitation Engineering, IEEE Transactions on* **12**(1), 24–31 (2004).

26. A. Hereid, S. Kolathaya, M. Jones, J. V. Why, J. Hurst, and A. Ames. "Dynamic Multi-Domain Bipedal Walking with ATRIAS through SLIP based Human-Inspired Control". *Proceedings of 17th ACM International Conference on Hybrid Systems: Computation and Control* 263–272 (2014).

27. P. Holmes, R. Full, D. Koditschek, and J. Guckenheimer. "The Dynamics of Legged Locomotion: Models, Analyses, and Challenges". *SIAM Rev.* **48**, 207–304 (2006). ISSN 0036-1445. doi: 10.1137/S0036144504445133.

28. D. Koepl, K. Kemper, and J. Hurst. "Force control for spring-mass walking and running". *Proceedings of IEEE/ASME International Conference on Advanced Intelligent Mechatronics* 639–644 (2010).

29. J. Rummel, Y. Blum, H. M. Maus, C. Rode, and A. Seyfarth. "Stable and robust walking with compliant legs". *Proceedings of IEEE International Conference on Robotics and Automation* 5250–5255 (2010).

30. C. Hubicki, J. Grimes, M. Jones, D. Renjewski, A. Spröwitz, A. Abate, and J. Hurst. "ATRIAS: Enabling Agile Biped Locomotion with a Template-Driven Approach to Robot Design". *Submitted to International Journal of Robotics Research* (2014).

31. A. Ames. "Human-inspired control of bipedal walking robots". *Automatic Control, IEEE Transactions on* **59**(5), 1115 – 1130 (2012).

32. S. Kolathaya, W. Ma, and A. Ames. "Composing Dynamical Systems to Realize Dynamic Robotic Dancing". *Proceedings of International Workshop on the Algorithmic Foundations of Robotics* (2014).

33. R. Murray, Z. Li, and S. Sastry. "A Mathematical Introduction to Robotic Manipulation". CRC Press Boca Raton (1994).

34. J. W. Grizzle, C. Chevallereau, R. W. Sinnet, and A. D. Ames. "Models, feedback control, and open problems of 3D bipedal robotic walking". *Automatica* **50**(8), 1955 – 1988 (2014).

35. A. Ames. "First Steps Toward Automatically Generating Bipedal Robotic Walking from Human Data". *Robotic Motion and Control 2011* **422**, 89–116 (2011).

36. R. Sinnet, M. Powell, R. Shah, and A. Ames. "A Human-Inspired Hybrid Control Approach to Bipedal Robotic Walking". *Proceedings of 18th IFAC World Congress* 6904–6911 (2011).

37. E. Westervelt, J. Grizzle, C. Chevallereau, J. Choi, and B. Morris. "Feedback Control of Dynamic Bipedal Robot Locomotion". CRC Press (2007).

38. B. Morris and J. Grizzle. "Hybrid invariance in bipedal robots with series compliant actuators". *Proceedings of 45th IEEE Conference on Decision and Control* 4793–4800 (2006).

39. A. Ramezani, J. W. Hurst, K. A. Hamed, and J. Grizzle. "Performance analysis and feedback control of ATRIAS, a 3D bipedal robot". *ASME Journal Dynamic Systems Measurement and Control* **136**(2) (2012).

40. H. Zhao, S. Nadubettu Yadukumar, and A. Ames. "Bipedal robotic running with partial hybrid zero dynamics and human-inspired optimization". *Proceedings of IEEE/RSJ International Conference on Intelligent Robots and Systems* 1821–1827 (2012).

41. S. N. Yadukumar, M. Pasupuleti, and A. Ames. "Human-Inspired Underactuated Bipedal Robotic Walking with AMBER on Flat-ground, Up-slope and Uneven Terrain". *IEEE International Conference on Intelligent Robots and Systems* (2012).

42. S. Sastry. "Nonlinear Systems: Analysis, Stability and Control". Springer New York (1999).

43. A. Ames, K. Galloway, J. Grizzle, and K. Sreenath. "Rapidly Exponentially Stabilizing Control Lyapunov Functions and Hybrid Zero Dynamics". *Automatic Control, IEEE Transactions on* **59**(4), 876 – 891 (2012).

44. B. Morris and J. Grizzle. "A Restricted Poincaré Map for Determining Exponentially Stable Periodic Orbits in Systems with Impulse Effects: Application to Bipedal Robots". *IEEE Conf. on Decision and Control* 4199 – 4206 (2005).

45. Y. Hürmüzlü and D.B. Marghitu. "Rigid body collisions of planar kinematic chains with multiple contact points". *IJRR* **13**(1), 82–92 (1994).

46. T. McGeer. "Passive Dynamic Walking". *IJRR* **9**(2), 62–82 (1990).